Copyright Warning & Restrictions

The copyright law of the United States (Title 17, United States Code) governs the making of photocopies or other reproductions of copyrighted material.

Under certain conditions specified in the law, libraries and archives are authorized to furnish a photocopy or other reproduction. One of these specified conditions is that the photocopy or reproduction is not to be "used for any purpose other than private study, scholarship, or research." If a, user makes a request for, or later uses, a photocopy or reproduction for purposes in excess of "fair use" that user may be liable for copyright infringement,

This institution reserves the right to refuse to accept a copying order if, in its judgment, fulfillment of the order would involve violation of copyright law.

Please Note: The author retains the copyright while the New Jersey Institute of Technology reserves the right to distribute this thesis or dissertation

Printing note: If you do not wish to print this page, then select "Pages from: first page # to: last page #" on the print dialog screen

ABSTRACT

DOMAIN DECOMPOSITION METHODS FOR THE SOLUTION OF MULTIPLE SCATTERING PROBLEMS

by
Michael Pedneault

This presents a Schur complement Domain Decomposition (DD) algorithm for the solution of frequency domain multiple scattering problems. Just as in the classical DD methods,(1) the ensemble of scatterers is enclosed in a domain bounded by an artificial boundary, (2) this domain is subdivided into a collection of nonoverlapping subdomains so that the boundaries of the subdomains do not intersect any of the scatterers, and (3) the solutions of the subproblems are connected via Robin boundary conditions matching on the common interfaces between subdomains. Subdomain Robin-to-Robin maps are used to recast the DD problem as a sparse linear system whose unknown consists of Robin data on the interfaces between subdomains—two unknowns per interface. The Robin-to-Robin maps are computed in terms of well-conditioned boundary integral operators. Unlike classical DD, the Domain Decomposition problem is not reformulated in the form of a fixed point iteration, but rather solved as a linear system through Gaussian elimination of the unknowns corresponding to inner interfaces between subdomains via Schur complements. Once all the unknowns corresponding to inner subdomains interfaces have been eliminated, a much smaller linear system involving solely the unknowns on the inner and outer artificial boundary is solved. The last section of this thesis offers numerical evidence that this Schur complement DD algorithm can produce accurate solutions for very large multiple scattering problems that are out of reach for other existing approaches.

DOMAIN DECOMPOSITION METHODS FOR THE SOLUTION OF MULTIPLE SCATTERING PROBLEMS

by
Michael Pedneault

A Dissertation
Submitted to the Faculty of
New Jersey Institute of Technology and
Rutgers, The State University of New Jersey – Newark
in Partial Fulfillment of the Requirements for the Degree of
Doctor of Philosophy in Mathematical Sciences

Department of Mathematical Sciences
Department of Mathematics and Computer Science, Rutgers-Newark

December 2018

APPROVAL PAGE

DOMAIN DECOMPOSITION METHODS FOR THE SOLUTION OF MULTIPLE SCATTERING PROBLEMS

Michael Pedneault

Catalin C. Turc, Dissertation Advisor — Date
Associate Professor, New Jersey Institute of Technology

Yassine Boubendir, Committee Member — Date
Professor, New Jersey Institute of Technology

Cyrill B. Muratov, Committee Member — Date
Professor, New Jersey Institute of Technology

Peter G. Petropoulos, Committee Member — Date
Associate Professor, New Jersey Institute of Technology

Francisco-Javier Sayas, Committee Member — Date
Professor, University of Delaware

BIOGRAPHICAL SKETCH

Author: Michael Pedneault

Degree: Doctor of Philosophy

Date: December 2018

Undergraduate and Graduate Education:

- Doctor of Philosophy in Mathematical Sciences,
  New Jersey Institute of Technology, Newark, NJ, 2018
- Master of Science in Financial Engineering,
  HEC Montreal, Montreal, Quebec, 2013
- Bachelor of Business Administration,
  University of Valencia, Valencia, Spain, 2011

Major: Mathematical Sciences

Presentations and Publications:

M. Pedneault, C. Turc and Y. Boubendir. (2017). Schur complement domain decomposition methods for the solution of multiple scattering problems. *IMA Journal of Applied Mathematics*, 82(5), 1104-1134.

M. Pedneault. Domain decomposition methods for the solution of multiple scattering problems. *SIAM Annual Conference*, Boston, July 2016.

I never saw a wild thing sorry for itself. A small bird will drop frozen dead from a bough without ever having felt sorry for itself.

D. H. Lawrence

ACKNOWLEDGMENT

I would like to thank my two good friends Dr. Catalin Turc and Dr. Yassine Boubendir for their tremendous support, the members of my committee Dr. Petropoulos, Dr. Muratov and Dr. Sayas for their constructive remarks and also the National Science Foundation for providing me with a research grant throughout my time at New Jersey Institute of Technology.

TABLE OF CONTENTS

Chapter **Page**

TABLE OF CONTENTS
(Continued)

Chapter **Page**

LIST OF TABLES

Table **Page**

LIST OF FIGURES

Figure **Page**

CHAPTER 1

FOUNDATIONS

Note to the reader: A lot of effort was given to make this thesis as much self-contained as possible, but should an avid reader want to, most of the survey material found in it can be supplemented by the excellent monographs Colton & Kress [30] and Martin [22] which contain comprehensive accounts of both theoretical and numerical developments in this field. I invite people to distribute this thesis whenever they see fit to the next generations of students who will carry on research on this specific topic, as it was written to address a lot of the technicalities that I personally had issues with when starting to work in the field for the first time. Also, note that for pedagogical purposes, you will find throughout this thesis little grey boxes like this one that are meant to encapsulate the results that are central to the development of the theory.

The numerical simulation of interaction of acoustic, electromagnetic, and elastic waves with large ensembles/clouds of scatterers, collectively referred to as multiple scattering, plays an important role in a variety of applied fields such as seismology, meteorology, remote sensing, and underwater acoustics, to name but a few.

At the heart of acoustic scattering, the Helmholtz equation $\Delta u + k^2 u = 0$ arises naturally from the wave equation $\Delta\phi = \frac{1}{c^2}\frac{\partial^2\phi}{\partial t^2}$ when the time dependence of the function $\phi(\mathbf{x}, t)$ is an harmonic function of circular frequency ω so that it can be written $\phi(\mathbf{x}, t) = Re(e^{-i\omega t}u(\mathbf{x}))$.

An attempt at solving this equation and a proper understanding of the kind of conditions to impose on the boundaries or at infinity calls for a basic knowledge of the quantities involved. We briefly review the physical background needed to

understand the scattering problem and although most of our work focuses on the two dimensional (2D) problem, it is easier to lay the foundations in three dimensions (3D) for sake of simplicity.

Consider an inviscid fluid medium at rest (no velocity flow $\mathbf{v}_0 = 0$) with uniform pressure p_0 and density ρ_0. Assume further that in this fluid the speed of sound is c. Acoustic waves are small perturbations of the medium's pressure $p(\mathbf{x}, t)$, density $\rho(\mathbf{x}, t)$ and velocity $\mathbf{v}(\mathbf{x}, t)$ so that these can be expressed as perturbations near their equilibrium states:

$$\begin{aligned} p(\mathbf{x}, t) &= p_0 + p_1(\mathbf{x}, t), \quad && p_1 \ll p_0 \\ \rho(\mathbf{x}, t) &= \rho_0 + \rho_1(\mathbf{x}, t), \quad && \rho_1 \ll \rho_0 \\ \mathbf{v}(\mathbf{x}, t) &= \mathbf{v}_1(\mathbf{x}, t), && |\mathbf{v}| \ll c = \sqrt{\frac{\partial p}{\partial \rho}|_{\rho_0}}. \end{aligned} \tag{1.1}$$

In all three equations we reiterated that the perturbations are small compared to their leading order equilibriums and that the velocity of the waves is much smaller than the speed of sound in the medium.

Understanding the behavior of acoustic waves hence amounts to finding the perturbations p_1, ρ_1 and $\mathbf{v}_1$. We must therefore establish a coherent system of relationships that these quantities must obey to and this is achieved by enforcing a set of fundamental physical laws in the underlying framework. Typically, to understand how a given physical law applies to a system, one first considers how it applies to a small, control volume, or "representative volume" which simply represents a small part of the system to which physical laws can be easily applied. In the following we establish the general relationship for conservative quantities.

1.1 The Mathematical Equations of Conservation Laws

Suppose V is an arbitrary control volume that is fixed in space and that q is a conservative quantity of interest inherent to V that can move or flow with volume density ρ measured in amount of q per unit volume. As V is fixed, if one observes what happens with q, the only way that it can change in time is by either fluxing it through the boundary ∂V or by creation inside of V. The flux of q, denoted $\mathbf{j}$, can be broken down further into two possibilities: conduction without the need of fluid transport (e.g. heat conduction in a solid) or actual transport along a fluid velocity field (e.g. mass) that flows freely across V. Denote by $\mathbf{d}$ the flux of q in the absence of transport and let $\mathbf{v}$ be the transport vector field so that the whole flux is understood as $\mathbf{j} = \mathbf{d} + \rho\mathbf{v}$. In addition, let us call σ the source (or sink) per unit of time per unit volume for q within V.

We then have that the rate of change of q in time can mathematically be expressed as:

$$\frac{dq}{dt} = \frac{d}{dt}\int_V \rho dV = -\int_{\partial V} \mathbf{j} \cdot d\mathbf{S} + \int_V \sigma dV. \tag{1.2}$$

In the above the minus sign accounts for the fact that the normal of ∂V , $\mathbf{n}$, is outward pointing so that quantities flowing opposite to $\mathbf{n}$ are actually inflows.

The surface integral is then converted into a volume integral using the divergence theorem:

$$\int_{\partial V} \mathbf{j} \cdot d\mathbf{S} = \int_V \nabla \cdot \mathbf{j} dV,$$

where $\nabla = (\frac{\partial}{\partial x}, \frac{\partial}{\partial y}, \frac{\partial}{\partial z})$ is the gradient operator. One can then reorganize and differentiate under the integral the LHS of (1.2) to get:

$$\int_V \left\{ \frac{\partial \rho}{\partial t} + \nabla \cdot \mathbf{j} - \sigma \right\} dV = 0.$$

Since V is arbitrary, it must be the case that the integrand vanishes everywhere, and that conclusion leads to the so called continuity equation:

$$\frac{\partial \rho}{\partial t} + \nabla \cdot \mathbf{j} - \sigma = 0. \tag{1.3}$$

The continuity equation is useful because both the mass and the momentum are conservative quantities that ought to solve equation (1.3) and more importantly, they involve the pressure, the density and the velocity field, which is what we seek. For instance if we consider the mass $m = \int_V \rho dV$ of what lies inside of V at a given time, as mass can only move with transport, $\mathbf{j} = \rho \mathbf{v}$, and can neither be created nor destroyed, $\sigma = 0$, we obtain the conservation of mass equation simply by replacing the appropriate terms:

$$\frac{\partial \rho}{\partial t} + \nabla \cdot (\rho \mathbf{v}) = 0. \tag{1.4}$$

The handling of the momentum $\mathbf{p} = \int_V \rho \mathbf{v} dV$ is done in a similar fashion although with the addition of a few technicalities. For example, the correct density to use for $\mathbf{p}$ is $\rho \mathbf{v}$ and as opposed to mass, momentum can flow without any transport vector field so that in this case one has to account for both sources of flux. The first one is being treated as before with the flux due to transport given by $(\rho \mathbf{v})\mathbf{v}^\top$ and one needs to look at the possible forces or stresses acting on ∂V to explain other changes in momentum. In general this is achieved by forming a stress tensor $\Sigma \in \mathbb{R}^{3\times 3}$ that captures sheer stresses (e.g. friction) off diagonal and normal stresses (e.g. pressure) on the diagonal making the full flux $\mathbf{j} = (\rho \mathbf{v})\mathbf{v}^\top + \Sigma$. Last but not least, if we want to be thorough, when gravity is accounted for there is effectively creation of momentum due to the gravitational pull in which case one has to set $\sigma = \rho \mathbf{g}$ where is $\mathbf{g}$ is the net acceleration.

Upon replacing in equation (1.3) we obtain the momentum conservation equation:

$$\frac{\partial \rho \mathbf{v}}{\partial t} + \nabla \cdot (\rho \mathbf{v}\mathbf{v}^\top + \Sigma) - \rho \mathbf{g} = 0. \tag{1.5}$$

Both equations (1.4) and (1.5) are nonlinear but can closely be approximated by linear ones using the order relations stated in equation (1.1) using the proxies $\rho \mathbf{v} \approx \rho_0 \mathbf{v}_1$ and $\mathbf{v}\mathbf{v}^\top = \mathbf{v_1}\mathbf{v_1}^\top \approx 0$. This is valid since the perturbations are assumed to be very small to start with, so their multiplications ought to be negligible. In addition, things can be simplified a bit further by neglecting gravity and by assuming there is no sheer stress and that the only normal force acting on ∂V is the pressure p so that the stress tensor reduces to $\Sigma_{ij} = p\delta_{ij}$. This simplification gives rise to the linearized mass conservation and momentum conservation equations:

$$\frac{\partial \rho_1}{\partial t} + \nabla \cdot (\rho_0 \mathbf{v_1}) = 0,$$

$$\rho_0 \frac{\partial \mathbf{v_1}}{\partial t} + \nabla p_1 = 0.$$

This system of equations is not uniquely solvable unless we append a third equation to close it. To do so we introduce the equation of state that ties the pressure and the density to each others. Specifically, one can draw from classical mechanics $c = \sqrt{\frac{dp}{d\rho}}$ implying that $p = p(\rho)$. When this relation holds, the fluid is referred to as barotropic. If we Taylor expand p to second order around its unperturbed state and use equation (1.1), we get:

$$\begin{aligned} p(\rho) &= p(\rho_0) + \frac{dp}{d\rho}|_{\rho_0}(\rho - \rho_0) + \mathcal{O}(\rho - \rho_0)^2 \\ &= p_0 + c^2\rho_1 + \mathcal{O}(\rho_1^2) \\ &\approx p_0 + c^2\rho_1. \end{aligned}$$

We can now use $p_1 \approx c^2 \rho_1$ as a third equation for a closed system:

$$\frac{\partial \rho_1}{\partial t} + \nabla \cdot (\rho_0 \mathbf{v_1}) = 0, \tag{1.6}$$

$$\frac{\partial \mathbf{v_1}}{\partial t} = -\frac{1}{\rho_0} \nabla p_1, \tag{1.7}$$

$$p_1 = c^2 \rho_1. \tag{1.8}$$

This can be solved as follows: first differentiate equation (1.6) with respect to t and use equation (1.7) in the result to get:

$$\frac{\partial^2 \rho_1}{\partial t^2} = \Delta p_1,$$

where $\Delta = \nabla \cdot \nabla$ is the Laplace operator. Then from equation (1.8) we obtain at once the wave equations for the density and the pressure:

$$\frac{1}{c^2} \frac{\partial^2 p_1}{\partial t^2} = \Delta p_1,$$
$$\frac{1}{c^2} \frac{\partial^2 \rho_1}{\partial t^2} = \Delta \rho_1,$$

and little work shows that the same equation holds for the velocity field as well

$$\frac{1}{c^2} \frac{\partial^2 \mathbf{v}_1}{\partial t^2} = \Delta \mathbf{v}_1. \tag{1.9}$$

It appears then that the behavior of acoustic waves is totally characterized by the wave equation only, for all three quantities of interest satisfy that equation. It is to be noted however that since the velocity is a vector field, equation (1.9) means that each components of $\mathbf{v}$ satisfy the scalar wave equation like the density

and pressure do. In order to avoid solving for each component individually, it is normally faster and simpler in practice to use the velocity potential ϕ for which $\nabla\phi = \mathbf{v}$. The potential also solves the scalar wave equation which can be verified upon substitution into equations (1.6), (1.7) and (1.8).

1.2 The Helmholtz Equation

From this point forward, we consider the scalar wave equation $\frac{1}{c^2}\frac{\partial^2\phi}{\partial t^2} = \Delta\phi$, where ϕ is left unspecified but for the most part should be thought of as a potential. If one uses separation of variables by looking for a solution of the form $\phi(\mathbf{x}, t) = \psi(t)u(\mathbf{x})$ we get:

$$\frac{1}{c^2}u\psi'' = \psi\Delta u,$$

which is reorganized into:

$$\frac{1}{c^2}\frac{\psi''}{\psi} = \frac{\Delta u}{u}.$$

Clearly, the only way that this can hold everywhere is that both sides be equal to the same constant, who we set to $-k^2$ for reasons that will be apparent soon. This separation of variables leads to two equations, a time dependent equation:

$$\psi'' + \omega^2\psi = 0,$$

whose solution is well known to be:

$$\psi = \alpha e^{-i\omega t} + \beta e^{i\omega t},$$

and an equation describing the space component known as the *Helmholtz equation*:

$$\Delta u + k^2 u = 0, \tag{1.10}$$

where we define $\omega := ck$ as the frequency and k as the wavenumber. In general, there is no closed-form solution to the Helmholtz equation except when it is assumed to be spherically symmetric. When this is the case, it can be verified using spherical coordinates that:

$$u = a\frac{e^{-ik|\mathbf{x}|}}{|\mathbf{x}|} + b\frac{e^{ik|\mathbf{x}|}}{|\mathbf{x}|}$$

is a solution to equation (1.10).

By combining the two solutions together, we see that the full solution to the spherical wave equation in its most general sense is:

$$\begin{aligned}\phi(\mathbf{x},t) =& \frac{a_1\cos(\omega t + k|\mathbf{x}|) + a_2\sin(\omega t + k|\mathbf{x}|)}{|\mathbf{x}|} + \frac{b_1\cos(\omega t - k|\mathbf{x}|) + b_2\sin(\omega t - k|\mathbf{x}|)}{|\mathbf{x}|} \\ =& \frac{1}{|\mathbf{x}|}f(t + |\mathbf{x}|/c) + \frac{1}{|\mathbf{x}|}g(t - |\mathbf{x}|/c),\end{aligned} \tag{1.11}$$

where $f = a_1\cos(\omega\cdot) + a_2\sin(\omega\cdot)$ and $g = b_1\cos(\omega\cdot) + b_2\sin(\omega\cdot)$ are used here as reminders of the classical d'Alembert's solution. It is well known that the function f describes *incoming waves* because the wave phases are given through $t + |\mathbf{x}|/c = const$ so that the wavefronts move towards the origin as time increases. Similarly the function g describes *outgoing waves* because the wave phases correspond to $t - |\mathbf{x}|/c = const$ and so the wavefronts are moving away from the origin with time. In either case these are sometimes referred to as monochromatic spherical wave.

It is important to note that we were able to distinguish between the incoming and outgoing solutions in the above thanks to having access to the full time-dependent solution. Yet it is generally the case, and especially for non-trivial

domains, that one will choose to solve independently the Helmholtz problem but will want to keep the ability to distinguish between outgoing and incoming waves; a task that may require some serious thinking without any insights of the time dependence. The following, which is due to Arnold Sommerfeld, presents a condition involving the spatial component u alone to determine whether it is outgoing or incoming.

1.2.1 The Sommerfeld Radiation Condition

The Sommerfeld Radiation Condition is a condition on the spatial component u for $|\mathbf{x}| \to \infty$ that allows one to distinguish between outgoing and incoming waves. It relies on the fact that from far away any kinds and/or configurations of sources can be *seen* as a single point-source (like a distant galaxy appears to us like a single star) so that one can draw asymptotic conclusions on general outgoing solutions by analyzing only spherically symmetric ones.

Perhaps the easiest way to derive the Sommerfeld Radiation Condition is to make a parallel between the d'Alembert's solution (1.11) and the otherwise popular Fourier transform solution. The Fourier transform comes about by choosing only one of the two available time solutions, say $\psi = \frac{1}{2\pi} e^{-i\omega t}$, together with a monochromatic spherical wave $u(\mathbf{x}|\omega)$ with parameter $\omega = ck$, that is $u(\mathbf{x}|\omega)$ solves the Helmholtz equation with $k = \omega/c$. One then argues that since ω was chosen arbitrarily in the first place when we performed the separation of variables, we might as well sum over all possible ω's (superposition principle) in order to get the most general form:

$$\phi(\mathbf{x}, t) = \frac{1}{2\pi} \int_{-\infty}^{\infty} e^{-i\omega t} u(\mathbf{x}|\omega) d\omega.$$

This equality indicates that there is a correspondence between u and ϕ through the Fourier transform. Indeed, using Fourier transforms terminology, if ϕ is the solution to the wave equation in the time domain, then it seems that u ought to

solve the wave equation in the frequency domain, that is; *the Helmholtz equation is the wave equation in the frequency domain.*

Of course, if we assume that we can perform the forward Fourier transform mapping the frequency domain to the time domain, then we could equally consider the inverse transform:

$$u(\mathbf{x}|\omega) = \int_{-\infty}^{\infty} e^{i\omega t}\phi(\mathbf{x}, t)dt.$$

Being able to convert the solution from the frequency domain to the time domain by a simple Fourier transform is a key observation for a few reasons. Clearly solving Helmholtz as opposed to the wave equation reduces the dimensionality of the problem by one degree and recovering the full solution in time is done very efficiently with the fast Fourier transform methods that are widely available.

If we now replace $\phi(\mathbf{x}, t)$ by its D'Alembert solution in the Fourier transform and letting $r = |\mathbf{x}|$, we get:

$$\begin{aligned} u(r|\omega) =& \frac{1}{r}\left(\int_{-\infty}^{\infty} e^{i\omega t} f(t + r/c)dt + \int_{-\infty}^{\infty} e^{i\omega t} g(t - r/c)dt\right) \\ =& \frac{1}{r}\left(\int_{-\infty}^{\infty} e^{i\omega(\tau - r/c)} f(\tau)d\tau + \int_{-\infty}^{\infty} e^{i\omega(\tau + r/c)} g(\tau)d\tau\right) \\ =& \frac{1}{r}e^{-ikr}\int_{-\infty}^{\infty} e^{i\omega\tau} f(\tau)d\tau + \frac{1}{r}e^{ikr}\int_{-\infty}^{\infty} e^{i\omega\tau} g(\tau)d\tau \\ =& \frac{1}{r}e^{-ikr}\hat{f}(\omega) + \frac{1}{r}e^{ikr}\hat{g}(\omega), \quad k = \omega/c. \end{aligned} \tag{1.12}$$

Looking at equation (1.12) we see that the general solution is the superposition of incoming waves, characterized by $e^{-ikr}\hat{f}(\omega)$, and outgoing waves characterized by $e^{ikr}\hat{g}(\omega)$. We seek to impose a condition on u alone that does not call for time insight and ensures that the solution be outgoing at infinity. The key is to consider linear combinations of $r\frac{\partial u}{\partial r} = -u - ike^{-ikr}\hat{f} + ike^{ikr}\hat{g}$ and $ikru = ike^{-ikr}\hat{f} + ike^{ikr}\hat{g}$ giving

the following relations:

$$r(\frac{\partial u}{\partial r} + iku) = -u + 2ike^{ikr}\hat{g},$$
$$r(\frac{\partial u}{\partial r} - iku) = -u - 2ike^{ikr}\hat{f}.$$

With the observation that $u \to 0$ with $r \to \infty$ it follows that indeed:

$$f = 0 \iff \lim_{r\to\infty} r(\frac{\partial u}{\partial r} - iku) = 0,$$
$$g = 0 \iff \lim_{r\to\infty} r(\frac{\partial u}{\partial r} + iku) = 0.$$

The condition $\lim_{r\to\infty} r(\frac{\partial u}{\partial r} - iku) = 0$ at infinity is known as the *Sommerfeld Radiation Condition* and ensures that the waves are outgoing and it needs to be imposed in the scattering problems for that reason. Similarly, a wave satisfying $\lim_{r\to\infty} r(\frac{\partial u}{\partial r} + iku) = 0$ will be an incoming wave. Note also that had we chosen $\psi = e^{i\omega t}$ earlier, the signs would have to be swapped in the condition in order to yield the same conclusion.

For other dimensions of interest, $d \in \{1, 2, 3\}$, a similar approach would show that the Sommerfeld condition reads $\lim_{r\to\infty} r^{\frac{d-1}{2}}(\frac{\partial u}{\partial r} - iku) = 0$.

A function that satisfies the Sommerfeld Radiation Condition is referred to as radiating, and from (1.12) we see that 3D radiating solutions satisfy $u \sim \frac{1}{r}e^{ikr}\hat{g}(\omega)$ when r gets large. We will later introduce the notion of *far field* behavior of u^s where we reserve a special name for the function $\hat{g}$, noting for now that it does not depend on r. For $d \in \{1, 2, 3\}$ we have the estimate $u \sim r^{\frac{1-d}{2}}e^{ikr}\hat{g}(\omega)$ as $r \to \infty$.

With the exception of an isotropic point scatterer problem, u will not obey (1.12) in bounded neighborhoods containing the origin, called the *near field*, since that equation was obtain from radially symmetrical problems (e.g. a unique source that radiates equally in all directions). The cases that we will consider in this work

are mostly for heterogeneous scatterers randomly arranged in space, meaning that in the surroundings of the arrangement, equation (1.12) will have little value to us. It will nonetheless retains its relevance in the far field for the intuitive reason recounted above.

1.3 The Boundary Conditions

This monograph is concerned with the behavior of *scattered waves* : waves that carry information *away* from a source (henceforth labelled u^s) in response to an incoming wave making contact with obstacles in space. This means that we will assume the knowledge of (1) the incoming wave, (also known as incident field or excitation source) and (2) the physical position of the obstacles (scatterers) making the unknown the quantity u^s.

So far, we have merely introduced the idea that scattered waves are those waves that are created at a source and then carry information away from it as time passes. Nothing has been said about the nature of the source and how it comes about. We have briefly mentioned the presence of objects called scatterers in the space in a misleading way that may have led the reader to believe that the scatterers themselves are sources, which would be inaccurate. Technically, for scattering waves to form on the surface of scatterers, we need the presence of an incident field (incoming, excitation wave) that impinges upon their boundary, which at this precise moment becomes the source that we have so far neglected to specify. In scattering problems this excitation field is assumed to be known by the observer, for in practice he is probably the one having control over it - *an observer sends a pulse in the hope of reading whatever comes back to him from the scatterers.* That incident field will henceforth be called u^{inc}.

Whether the shapes and locations of the scatterers are known give rise to two distinct problems: direct versus inverse. Inverse problems are concerned with reconstructing the scatterers and their properties from the readings of the far

field. Different scatterers have different signatures. A trivial example could be that someone wants to map the sea floor by emitting acoustic pulses and taking measurements of the time it takes the signal to come back so that the depth can be measured.

In direct problems, it is the acoustic response that is unknown but all the information regarding the scatterers, like their location, composition and shape is available. Once again one would have the task to emit an acoustic signal and record the readings. This work will be dedicated only to direct acoustic scattering, meaning that we will always have all the information regarding the scatterers readily available. This also means that we will have to mathematically describe the behavior that is expected from the excitation field once it makes contact with the boundaries of the scatterers. Different types of boundary composites ought to yield different responses in both phases and magnitude. Indeed, if an object's boundary allows the wave to be partially absorbed, then the reflected field won't be as strong as one that would be totally reflected. Hence, two scatterers can share the same shape, and yet reflect the incident field in different manners due to having different materials properties. This is because sound waves can be reflected in essentially two ways depending on whether the boundary is soft or hard.

Boundaries that are made of sound-soft material have a very low acoustic impedance compared to the acoustic impedance of the carrier medium, (i.e. $[\rho c]^- \ll [\rho c]^+$). When an incident wave impinges on them, a scattered wave of the same magnitude but with opposite polarity is instantaneously created. Mathematically, this is easily expressed as:

$$u^s = -u^{inc} \quad \text{on} \quad \Gamma,$$

or equivalently as:

$$u := u^s + u^{inc} = 0 \quad \text{on} \quad \Gamma,$$

where Γ is an arbitrary soft-sound boundary, u^s is the scattered response and u^{inc} is the excitation field. Note that this notation will be used extensively in this work from now on and that by $u = u^s + u^{inc}$ we will imply the total field.

Whenever there is no ambiguity, we may occasionally refer to these boundary conditions as *Dirichlet Boundary Condition* . As an example, sound travels at 343 m/s in air with density 1.204 kg/m^3 while it travels at 5,000 m/s in steel with density of 8,050 kg/m^3. This accounts for an acoustic impedance of 413.3 Pa $\cdot$ s/m for the air and 40,250,000 Pa$\cdot$ s/m for the steel and consequently one would have to use Dirichlet boundary conditions to study the sound propagation inside of a metallic object that is surrounded by air.

Cases where the surrounding medium has a much lower acoustic impedance compared to the boundary of the object are called sound-hard ($[\rho c]^- \gg [\rho c]^+$). When this happens the correct boundary formulation to impose is:

$$\frac{\partial u^s}{\partial n} = -\frac{\partial u^{inc}}{\partial n} \quad \text{on} \quad \Gamma,$$

or equivalently

$$\frac{\partial u}{\partial n} = 0 \quad \text{on} \quad \Gamma,$$

and is known as *Neumann Boundary Condition.* As the incident field undergoes a jump from low speed (or low potential) to high speed (potential), this results in an instantaneous opposite loss in the response and that is what the condition entails.

In general, one can impose the so called *Robin Boundary Condition,* or *Impedance* ; a condition that is somewhat between the sound-hard and sound-soft

one by introducing an admittance parameter $\lambda \in \mathbb{R}$:

$$\frac{\partial u}{\partial n} + i\lambda u = 0 \quad \text{on} \quad \Gamma.$$

It is easy to see that the limiting cases $\lambda \to \infty$ and $\lambda \to 0$ yield the Dirichlet and Neumann cases, respectively. In Chapter 2, we officially begin studying the exterior scattering problem in 2D.

CHAPTER 2

SCATTERING REVIEW IN 2D

In this chapter, we briefly review the theory that is essential to understanding and solving the simple case of acoustic scattering in the exterior of a simply connected region in 2D. We would expect anyone who has completed a first semester in PDEs and Numerical Methods to know that there are several solution techniques to most problems, both theoretically and numerically. We hereby provide a solution in terms of boundary integral equations as we believe it to be the best suited method for our needs in exterior domains. More will be said later regarding that choice when we enter the gist of Domain Decomposition.

2.1 The Scattering of Acoustic Waves

Let S be a closed, bounded and simply connected region in $\mathbb{R}^2$ with a soft-sound boundary Γ. We wish to compute the scattered wave u^s in the exterior domain $\mathbb{R}^2 - \bar{S}$ that is formed when an incoming plane wave $u^{inc}(\mathbf{x}) = e^{ik\mathbf{x}\cdot\mathbf{d}}$ travelling in direction $\mathbf{d}$ with wavenumber k impinges upon Γ. Following the discussion of Chapter 1, the problem is formulated as:

The Scattering Problem

$$\begin{aligned} (\Delta + k^2)u^s &= 0 \quad \text{in} \quad \mathbb{R}^2 - \bar{S}, \\ u^s &= -u^{inc} \quad \text{on} \quad \Gamma, \\ r^{\frac{1}{2}}\left(\frac{\partial u^s}{\partial r} - iku^s\right) &\to 0 \quad \text{as} \quad r = |\mathbf{x}| \to \infty. \end{aligned} \tag{2.1}$$

For a proof of existence and uniqueness of the solution to the Helmholtz problem, we refer to Colton & Kress [30].

As we will employ boundary integral representations of the solution, we now present the relevant integral kernels that will be used throughout this thesis.

2.1.1 The Fundamental Solution

The radiating fundamental solution $G_k(\mathbf{x}-\mathbf{y})$ (or Green's function) to the Helmholtz equation in 2D is the function that solves:

$$\Delta_{\mathbf{x}} G_k + k^2 G_k = -\delta(\mathbf{x}-\mathbf{y}), \quad \mathbf{x},\mathbf{y} \in \mathbb{R}^2,$$
$$r^{\frac{1}{2}} \left(\frac{\partial G_k}{\partial r} - ikG_k \right) \to 0 \quad \text{as} \quad r = |\mathbf{x}-\mathbf{y}| \to \infty,$$

where $\Delta_{\mathbf{x}}$ is the Laplacian with respect to $\mathbf{x}$ and δ is the Dirac delta distribution. It is given by the expression

$$G_k(\mathbf{x}-\mathbf{y}) := \frac{i}{4} H_0^{(1)}(k|\mathbf{x}-\mathbf{y}|),$$

where $H_0^{(1)} = J_0 + iY_0$ is the Hankel function of the first kind and J_0, Y_0 are the Bessel functions of order 0 given by:

$$J_0(x) := \sum_{m=0}^{\infty} (-1)^m \frac{1}{2^{2m}(m!)^2} x^{2m},$$
$$Y_0(x) := \frac{2}{\pi} \left(\ln \frac{x}{2} + \gamma \right) J_0(x) - \frac{2}{\pi} \sum_{m=1}^{\infty} a_{2m} H_m x^{2m}.$$

$H_m := \sum_{j=1}^{m} \frac{1}{j}$ is the mth harmonic number, $a_{2m} := (-1)^m \frac{1}{2^{2m}(m!)^2}$ and $\gamma = \lim_{m\to\infty} (H_m - \ln m) = 0.5772...$ is the Euler Mascheroni constant. The details of the construction of the Green's function can be found in Appendix A at the end of this thesis.

For the asymptotic behaviors of the fundamental solution as $\mathbf{x} \to \mathbf{y}$ and $\mathbf{x} \to \infty$, it can be showed that:

$$G_k(\mathbf{x}-\mathbf{y}) = \frac{1}{2\pi}\log\frac{1}{|\mathbf{x}-\mathbf{y}|} + \mathcal{O}(1) \text{ as } \mathbf{x} \to \mathbf{y}$$

and that:

$$G_k(\mathbf{x}-\mathbf{y}) = \frac{e^{i\pi/4}}{\sqrt{8\pi k}}\frac{e^{ik|\mathbf{x}-\mathbf{y}|}}{\sqrt{|\mathbf{x}-\mathbf{y}|}} + \mathcal{O}\big(|\mathbf{x}-\mathbf{y}|^{-3/2}\big) \text{ as } \mathbf{x} \to \infty.$$

This estimate can equally be expressed in terms of $|\mathbf{x}|$ alone using the polar coordinates $\mathbf{x} \sim (|\mathbf{x}|, \theta)$ and $\mathbf{y} \sim (|\mathbf{y}|, \phi)$, $\psi := \theta - \phi$ and the fact that $|\mathbf{y}|\cos\psi = \hat{\mathbf{x}} \cdot \mathbf{y}$ where we have set $\hat{\mathbf{x}} = \frac{\mathbf{x}}{|\mathbf{x}|}$:

$$\begin{aligned}
|\mathbf{x}-\mathbf{y}| &= \sqrt{|\mathbf{x}|^2 - 2|\mathbf{x}||\mathbf{y}|\cos\psi + |\mathbf{y}|^2} \\
&= |\mathbf{x}|\sqrt{1 - 2\frac{|\mathbf{y}|}{|\mathbf{x}|}\cos\psi + \frac{|\mathbf{y}|^2}{|\mathbf{x}|^2}} \\
&= |\mathbf{x}| - |\mathbf{y}|\cos\psi + \mathcal{O}(|\mathbf{x}|^{-1}) \\
&= |\mathbf{x}| - \hat{\mathbf{x}} \cdot \mathbf{y} + \mathcal{O}(|\mathbf{x}|^{-1}).
\end{aligned}$$

Using this expansion and the fact that $|\mathbf{x}-\mathbf{y}| \sim |\mathbf{x}|$ in the above asymptotic for $|\mathbf{x}| \to \infty$ gives the following expression that should be reminiscent from Section 1.2.1 and will be used again shortly for the far field pattern.

$$G_k(\mathbf{x}-\mathbf{y}) = \frac{e^{ik|\mathbf{x}|}}{\sqrt{|\mathbf{x}|}}\frac{e^{i\pi/4}}{\sqrt{8\pi k}}e^{-ik\hat{\mathbf{x}}\cdot\mathbf{y}} + \mathcal{O}\big(|\mathbf{x}|^{-3/2}\big) \text{ as } \mathbf{x} \to \infty. \tag{2.2}$$

We next cite the integral operators that are inherent to the Green's function.

2.1.2 The Layer Potentials and Boundary Operators

Let Γ be a closed curve in $\mathbb{R}^2$ that encloses a bounded domain Ω. For a given density φ defined on Γ we define the *single layer potential* in the form:

$$[SL_\Gamma\varphi](\mathbf{x}) := \int_\Gamma G_k(\mathbf{x}-\mathbf{y})\varphi(\mathbf{y})ds(\mathbf{y}), \qquad \mathbf{x}\in\mathbb{R}^2\backslash\Gamma,$$

and the *double layer potential*:

$$[DL_\Gamma\varphi](\mathbf{x}) := \int_\Gamma \frac{\partial G_k(\mathbf{x}-\mathbf{y})}{\partial \mathbf{n}(\mathbf{y})}\varphi(\mathbf{y})ds(\mathbf{y}), \qquad \mathbf{x}\in\mathbb{R}^2\backslash\Gamma,$$

where $\mathbf{n}$ denotes the unit normal to Γ pointing toward the exterior domain $\mathbb{R}^2 \setminus \Omega$.

By letting $\mathbf{x}\to\Gamma$, we introduce an additional four boundary integral operators associated with the Helmholtz equation. These are formally understood through the applications of Dirichlet and Neumann traces on Γ to the single and double layer operators defined above. We note the exterior Dirichlet and Neumann traces on Γ by $\gamma_\Gamma^{D,1}$ and $\gamma_\Gamma^{N,1}$ and the interior Dirichlet and Neumann traces on Γ, respectively by $\gamma_\Gamma^{D,2}$ and $\gamma_\Gamma^{N,2}$ (both Neumann traces are taken with respect to the exterior normal $\mathbf{n}$). Applying these traces to the single and double layer potentials we obtain:

$$\begin{aligned}
&\gamma_\Gamma^{D,1}SL_\Gamma\varphi = \gamma_\Gamma^{D,2}SL_\Gamma\varphi = V_\Gamma\varphi,\\
&\gamma_\Gamma^{N,j}SL_\Gamma\varphi = (-1)^j\frac{\varphi}{2} + K_\Gamma^\top\varphi, \quad j=1,2,\\
&\gamma_\Gamma^{D,j}DL_\Gamma\varphi = (-1)^{j+1}\frac{\varphi}{2} + K_\Gamma\varphi, \quad j=1,2,\\
&\gamma_\Gamma^{N,1}DL_\Gamma\varphi = \gamma_\Gamma^{N,2}DL_\Gamma\varphi = D_\Gamma\varphi.
\end{aligned}$$

The operators K_Γ and $K_\Gamma^\top$, usually referred to as *double and adjoint double layer operators*, are defined for a given wavenumber k and density φ as:

$$[K_\Gamma\varphi](\mathbf{x}) := \int_\Gamma \frac{\partial G_k(\mathbf{x}-\mathbf{y})}{\partial \mathbf{n}(\mathbf{y})}\varphi(\mathbf{y})ds(\mathbf{y}),\ \mathbf{x} \text{ on } \Gamma,$$

and:

$$[K_\Gamma^\top\varphi](\mathbf{x}) := \int_\Gamma \frac{\partial G_k(\mathbf{x}-\mathbf{y})}{\partial \mathbf{n}(\mathbf{x})}\varphi(\mathbf{y})ds(\mathbf{y}),\ \mathbf{x} \text{ on } \Gamma.$$

Furthermore, for a given wavenumber k and density φ, the *hypersingular operator* [1] D_Γ denotes the Neumann trace of the double layer potential on Γ given in terms of a Hadamard Finite Part (FP) integral which can be re-expressed in terms of a Cauchy Principal Value (PV) integral that involves the tangential derivative ∂_s on the curve Γ:

$$\begin{aligned}[D_\Gamma\varphi](\mathbf{x}) :=& \text{FP}\int_\Gamma \frac{\partial^2 G_k(\mathbf{x}-\mathbf{y})}{\partial \mathbf{n}(\mathbf{x})\partial \mathbf{n}(\mathbf{y})}\varphi(\mathbf{y})ds(\mathbf{y}) \\ =& k^2\int_\Gamma G_k(\mathbf{x}-\mathbf{y})(\mathbf{n}(\mathbf{x})\cdot\mathbf{n}(\mathbf{y}))\varphi(\mathbf{y})ds(\mathbf{y}) + \\ & \text{PV}\int_\Gamma \partial_s G_k(\mathbf{x}-\mathbf{y})\partial_s\varphi(\mathbf{y})ds(\mathbf{y}).\end{aligned}$$

Finally, the *single layer operator* V_Γ is defined as:

$$[V_\Gamma\varphi](\mathbf{x}) := \int_\Gamma G_k(\mathbf{x}-\mathbf{y})\varphi(\mathbf{y})ds(\mathbf{y}),\ \mathbf{x} \text{ on } \Gamma,$$

for a density function φ defined on Γ.

[1] Given an integral of the form $\int_{\mathbb{R}^n} K(x,y)f(y)dy$ for some smooth function f that is compactly supported and a kernel K. If $|K(x,y)| \sim |x-y|^{-\alpha}$ as $x \to y, \alpha > 0$, the kernel is said to be *singular* because it tends to infinity on the diagonal. Singular kernels are further classified into either *weakly singular* ($\alpha < n$) as their integrand is absolutely summable (i.e. $\in L^1(\mathbb{R}^n)$), or *hypersingular* ($\alpha > n$) when the estimate on $|K|$ does not guaranty convergence. When this happens, the integrals are understood in the sense of principal value.

2.2 The Green's Identities and the Representations of Solutions

We briefly review the Green's identities as these will come handy for the reminder of this thesis.

Let Ω be a simply connected and bounded region in $\mathbb{R}^2$ with a C^2 boundary Γ and let $\mathbf{F}(\mathbf{x}) \in C^1(\bar{\Omega})^3$ be a vector-valued function. If $\mathbf{n}$ is the outward pointing unit normal vector to Γ, the divergence theorem states that:

$$\int_\Omega \text{div}\mathbf{F}(\mathbf{x})d\mathbf{x} = \int_\Gamma \mathbf{F}(\mathbf{x}) \cdot \mathbf{n}(\mathbf{x})ds(\mathbf{x}).$$

If for $u, v \in C^2(\bar{\Omega})$ we let $\mathbf{F}(\mathbf{x}) = u(\mathbf{x})\nabla v(\mathbf{x})$, the divergence theorem gives *Green's first identity*:

$$\int_\Omega (u\Delta v + \nabla u \cdot \nabla v)d(\mathbf{x}) = \int_\Gamma u\frac{\partial v}{\partial \mathbf{n}}ds(\mathbf{x}).$$

Similarly, for $\mathbf{F}(\mathbf{x}) = v(\mathbf{x})\nabla u(\mathbf{x})$,

$$\int_\Omega (v\Delta u + \nabla v \cdot \nabla u)d(\mathbf{x}) = \int_\Gamma v\frac{\partial u}{\partial \mathbf{n}}ds(\mathbf{x}).$$

The *Green's second identity* is obtained from a simple subtraction of the last two equations:

$$\int_\Omega (u\Delta v - v\Delta u)d(\mathbf{x}) = \int_\Gamma \left(u\frac{\partial v}{\partial \mathbf{n}} - v\frac{\partial u}{\partial \mathbf{n}}\right) ds(\mathbf{x}).$$

The following theorem is extremely valuable as it allows solutions to the Helmholtz equation to be represented using boundary integrals. For a proof we refer to Colton & Kress [30].

Theorem 1. *(Green's formula). Let S be as before with boundary Γ and $u^s \in C^2(\mathbb{R}^2\backslash\bar{S}) \cap C^1(\mathbb{R}^2\backslash S)$ be a radiating solution of the Helmholtz equation in the exterior of S and $G_k(\mathbf{x}-\mathbf{y})$ be the corresponding Green's function. Then for $\mathbf{x} \in \mathbb{R}^2\backslash\bar{S}$,*

$$u^s(\mathbf{x}) = \int_\Gamma \left(u^s(\mathbf{y}) \frac{\partial G_k(\mathbf{x}-\mathbf{y})}{\partial \mathbf{n}(\mathbf{y})} - G_k(\mathbf{x}-\mathbf{y}) \frac{\partial u^s(\mathbf{y})}{\partial \mathbf{n}(\mathbf{y})} \right) ds(\mathbf{y}). \tag{2.3}$$

In particular if u^s is a solution to equation (2.1), then this expression reduces to:

$$u^s(\mathbf{x}) = -[SL_{\partial S}\partial_n u^s](\mathbf{x}), \quad \mathbf{x} \in \mathbb{R}^2 \setminus S. \tag{2.4}$$

Applying the exterior Dirichlet and Neumann traces (the latter we denote simply by ∂_n) to equation (2.4) we obtain the classical boundary integral equation of the first kind:

$$V_{\partial S}\partial_n u^s = u^{inc}, \tag{2.5}$$

and respectively the boundary integral equation of the second kind:

$$\frac{1}{2}\partial_n u^s + K^\top_{\partial S}\partial_n u^s = \frac{1}{2}\partial_n u^{inc}. \tag{2.6}$$

Unfortunately, neither formulation (2.6) nor (2.5) is equivalent to the original scattering problems for all wavenumbers k. Classical Fredholm arguments can be used to show that these equations fail to be invertible for values of the wavenumber k that coincide with eigenvalues of the Laplacian in the domain S with Dirichlet or Neumann vanishing boundary conditions on ∂S. The fix is to use a linear

combination of equations (2.6) and (2.5) of the form:

$$[I + 2K_{\partial S}^{\top} - 2i\eta V_{\partial S}]\partial_n u^s = \partial_n u^{inc} - 2i\eta u^{inc}, \eta \in \mathbb{R},\ \eta \neq 0, \tag{2.7}$$

that is referred to as the Combined Field Integral Equation (CFIE). The CFIE formulation is uniquely solvable for any wavenumber k. The complex value $i\eta$ in equation (2.7) is related to impedance boundary value problems in the domain S which, unlike Dirichlet or Neumann boundary value problems for the Helmholtz equation, are uniquely solvable for all wavenumbers k.

For the case when S is an open arc, the formulas above have to be modified accordingly. In that case there are two normals $\mathbf{n}_+$ and $\mathbf{n}_-$ on S, and it can be shown that the scattered field can be represented as:

$$u^s(\mathbf{x}) = -[SL_S(\partial_{n_+} u^s - \partial_{n_-} u^s)](\mathbf{x}), \quad \mathbf{x} \in \mathbb{R}^2 \setminus S,$$

leading to the boundary integral equation of the first kind:

$$V_S(\partial_{n_+} u^s - \partial_{n_-} u^s) = u^{inc} \quad \text{on } S. \tag{2.8}$$

The integral equation (2.8) is uniquely solvable for all wavenumbers k. We note that it is not possible to derive integral equations of the second kind in the case when the scatterer S is an open arc.

For asymptotic estimates on the solution of the Helmholtz problem, we can combine equations (2.2) and (2.3) to get the following far field leading order term:

$$u^s(\mathbf{x}) = \frac{e^{ikr}}{\sqrt{r}} u_\infty(\hat{\mathbf{x}}; \mathbf{d}) + \mathcal{O}(r^{-3/2}),$$

where $r = |\mathbf{x}|, \hat{\mathbf{x}} = \frac{\mathbf{x}}{|\mathbf{x}|}$ and where the quantity $u_\infty(\hat{\mathbf{x}}; \mathbf{d})$ is defined here:

Definition: We define the quantity:

$$u_\infty(\hat{\mathbf{x}}; \mathbf{d}) = \frac{e^{i\pi/4}}{\sqrt{8\pi k}} \int_\Gamma \left(u^s(\mathbf{y}) \frac{\partial e^{-ik\hat{\mathbf{x}}\cdot\mathbf{y}}}{\partial \mathbf{n}(\mathbf{y})} - \frac{\partial u^s(\mathbf{y})}{\partial \mathbf{n}(\mathbf{y})} e^{-ik\hat{\mathbf{x}}\cdot\mathbf{y}} \right) ds(\mathbf{y})$$

as the far field pattern of u^s corresponding to the incident field $e^{ik\mathbf{x}\cdot\mathbf{d}}$.

Note: From a practical standpoint, one may opt for the use of an ansatz:

$$u^s(\mathbf{x}) = [(DL_{\partial S} - i\eta SL_{\partial S})\varphi](\mathbf{x}), \quad \mathbf{x} \in \mathbb{R}^2 \setminus S,$$

when dealing with closed obstacles.

An application of the Dirichlet trace to it yields the boundary integral equation of the second kind:

$$(I + 2K_{\partial S} - 2i\eta V_{\partial S})\varphi = -2u^{inc} \quad \text{on } \partial S.$$

This equation is equivalent to (2.7) since $\sigma(K) = \sigma(K^\top)$ over the eigenvalues of the Laplacian operator (for being real), making this equation uniquely solvable for all wavenumbers k.

Similarly, for open obstacles the use of the representation:

$$u^s(\mathbf{x}) = -[SL_S\varphi](\mathbf{x}), \quad \mathbf{x} \in \mathbb{R}^2 \setminus S,$$

works just as well with corresponding equation:

$$V_S\varphi = u^{inc} \quad \text{on } S,$$

which is clearly equivalent to equation (2.8).

CHAPTER 3

DOMAIN DECOMPOSITION METHODS FOR MULTIPLE SCATTERING PROBLEMS IN 2D

3.1 The Challenges Associated with Multiple Scattering

While the direct extension of single scatterer solvers to multiple scatterers is in principle straightforward, solvers in the latter case are confronted by considerably larger-sized problems that exhibit increasingly worse conditioning properties which can be attributed to the need to resolve complicated multiple reflections between scatterers. The level of difficulty associated with the problem is also highly dependent on the configuration of the computational domain and in many cases proves to become increasingly challenging to solve for non-Lipschitz objects.

In addition to being greatly affected by the smoothness attributes of the boundary alone, the exterior variant of the Helmholtz problem renders most classical volumetric methods such as finite differences and finite elements at best inefficient on account of the size of the unknown's vector, regardless of how nice the scatterers may be. These methods further handicap themselves in having to deal with the Sommerfeld radiation condition on the boundary of the truncated domain. This requires using on the edge of the truncated domain local boundary operators such as the Absorbing Boundary Conditions (ABC) or the Perfectly Matched Layers (PML) to mimic a phenomenon that only holds true at infinity, introducing approximation errors in addition to the aforementioned issue of choking on large domains.

Boundary Integral Equations (BIE) effectively reduce the dimensionality of the problem in addition to automatically enforcing the radiation condition through the Green's function. They enjoy no drawback with respect to unbounded domains and for that reason it should not be surprising that these are greatly favored over the classical volumetric discretization methods. But while BIE methods certainly present some cost savings, they too can easily be bottlenecked for multiple

scattering configurations where the computational domain potentially comprises a large number of scatterers. The number of unknowns N can often go north of 10^4 and the CPU cost of solving such a system via a direct method like LU or QR decomposition is $\mathcal{O}(N^3)$ which exceeds, or heavily constrains, what personal computers can handle. This then drives users to settle for iterative scheme like Krylov subspaces solvers.

Krylov subspace iterative solvers for the associated linear algebra problems can be fast in some cases (e.g., Laplace with $k = 0$) but their performance is well known to deteriorate as k gets larger and are rarely used on their own in high frequency regime problems as they typically require very large numbers of iterations. Although certain preconditioning strategies can alleviate this issue to some extent in the diffuse case (e.g. when the distances between scatterers are large with respect to the wavelength of the probing incident wave) [2, 3], general purpose preconditioners that work effectively throughout the frequency range are difficult to construct for boundary integral solvers for multiple scattering problems.

On account of these limitations, the solution of multiple scattering problems involving large ensembles of scatterers has been approached through various approximations that render the computations tractable yet do not control the errors incurred. One of the most popular approaches is the Lax-Foldy method [11, 21] in which a multiple scattering scheme is set up to account for contributions on any one of the scatterers by the rest of the scatterers wherein the scatterers are replaced by point isotropic scatterers.

Another widely used algorithm for solution of multiple scattering problems is the T-matrix method pioneered by Waterman [29]. The main idea in this method is to use particular solutions of Helmholtz equation to construct functional bases for incoming fields and outgoing (i.e., radiative) fields and to assign an operator between incoming fields impinging on a given scatterer and fields scattered by it using decompositions in those incoming/outgoing bases. This operator describes

completely the geometrical and material properties of a single scatterer. Using the T-matrix framework, the solution of multiple scattering problems consists of combining the T-matrices for each individual scatterer in the ensemble in a large linear system. Truncated T-matrices can be computed by null-fields methods [29] or more reliably and whenever possible by boundary integral equation methods [17, 22, 20]. However, the T-matrix method that uses spherical multipole expansions suffers from numerical instabilities associated with fast growth of Hankel functions [22], and it was only recently that robust bases functions for T-matrix methods have been proposed and analyzed [13].

Our approach to the multiple scattering problem is to use Domain Decomposition Methods (DDM), a divide and conquer strategy for solution of large-sized problems whose direct solutions is too costly or out of reach to existing resources.

3.2 The Domain Decomposition Method

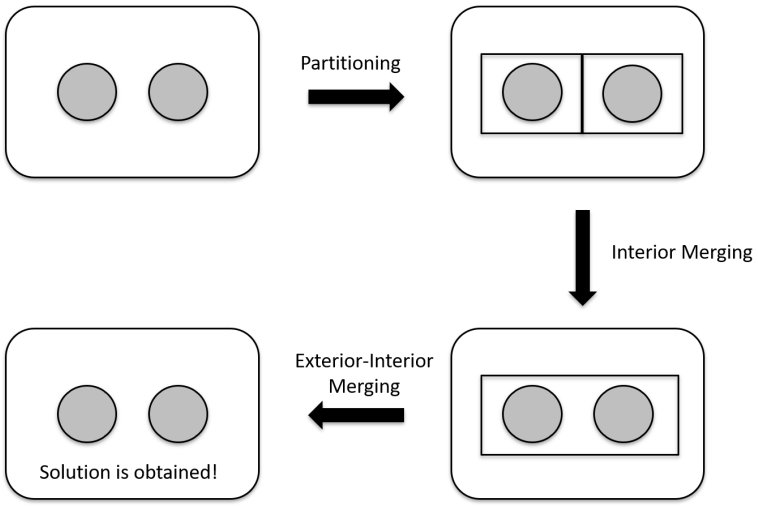

Figure 3.1 Domain decomposition steps.

In a nutshell, DDM decompose the original problem (typically associated to a PDE) to be solved in a certain computational domain into subproblems associated to subdomains, so that each subproblem can be solved efficiently with existing methods.

Although in this text we will decompose the domain into a collection of non-overlapping subdomains, it is worth pointing out that this need not be the case, and as a matter of fact did not originated as such. Hermann Schwarz was the first to allude the idea in 1869 while working on a way to prove the Dirichlet's Principle, which in turn was key to Riemann for proving his mapping theorem for complex analytic functions. Schwarz developed an alternating iterative method to solve the Dirichlet problem in the union of two overlapping domains, as shown by his original sketch of a domain decomposition depicted below. The idea was rather simple: solve each original PDE in its own domain successively while passing the Dirichlet data as updated boundary conditions at each step between subdomains.

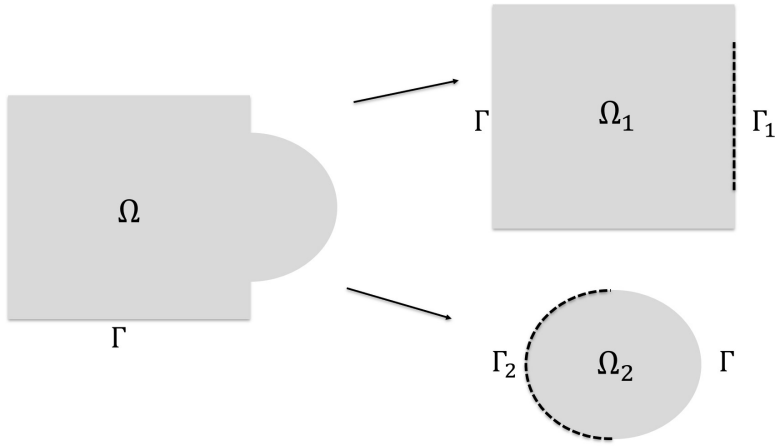

Figure 3.2 Original idea of overlapping domain decomposition.

The method was specifically designed to solve the Laplace equation:

$$\Delta u_1^{n+1} = 0 \quad \text{in} \quad \Omega_1, \qquad \Delta u_2^{n+1} = 0 \quad \text{in} \quad \Omega_2,$$
$$u_1^{n+1} = u_2^n \quad \text{on} \quad \Gamma_1, \qquad u_2^{n+1} = u_1^{n+1} \quad \text{on} \quad \Gamma_2.$$

It is important to note that this example is only of theoretical interest. By now people are well aware of the limitations of the classical Schwarz alternating scheme stated above for the Helmholtz problem with high wave numbers, not to mention that the rate of convergence is tied to the size of the overlap, leading to redundant effort in most cases.

In light of this observation, a good amount of attention has been given to finding new methods based on non-overlapping subdomains in the late 1980s. The most notorious one is due to Pierre-Louis Lions in his 1989 paper *On the Schwarz Alternating Method III: A Variant for Nonoverlapping Subdomains.* At around the same time Bruno Despres independently proposed the same method in his PhD thesis. In there he suggested a variant of the classical Schwarz alternating method that had two key distinctions: No more overlapping was required and Robin data $\frac{\partial u_i^n}{\partial \mathbf{n}_i} + \lambda u_i^n, \quad (i = 1, 2), \lambda > 0$ was now used instead of Dirichlet u_i in the boundary conditions at each step. Beside the obvious reasons for wanting to ditch the overlapping, they were now able to prove the convergence of the algorithm using energy estimates.

In this thesis, we apply the DD strategy to multiple scattering problems by enclosing the ensemble/cloud of scatterers in a domain bounded by an artificial boundary, and we proceed by subdividing this domain into a collection of nonoverlapping subdomains so that the (artificial) boundaries of the subdomains do not intersect any of the scatterers. The original scattering problems is thus decomposed into a sequence of multiple scattering subproblems in each of the subdomains. Once the domain has been partitioned into non-overlapping subregions, the corresponding subproblems are solved independently in terms of unknowns pertaining to the interface boundaries, which are then coupled in a global system. In the context of non-overlapping methods, the coupling between adjacent subproblems is realized via transmission conditions imposed on the artificial interfaces separating them and the choice of transmission conditions and their implementation is central to the success of the method. Following the prior discussion, it is now common practice in DD to go for Robin data as the choice of transmission conditions on the common interfaces between subdomains [7].

The central component of our algorithm is the use of Robin-to-Robin isometric operators that map outgoing Robin information to incoming information for

subdomain problems that involve a collection of scatterers enclosed by an artificial boundary. The Robin data is exchanged through the maps on the artificial boundary and physically relevant boundary conditions are imposed on the scattererss. We use these Robin-to-Robin maps associated to each of the subdomains to recast the DD formulation for the solution of the multiple scattering problem into the form of a linear system whose unknown consists of global Robin data defined on the interfaces between subdomains—two unknowns per each interface. The idea of using Robin-to-Robin maps as robust alternative to the more popular Dirichlet to Neumann maps can be traced back to the work [18] where it was used to good effect for calculations involving periodic waveguides containing defects/perturbations; see also [10] for a more recent application to computation of guided modes in photonic crystal waveguides.

Once each subdomain Robin-to-Robin map is computed, we proceed with the hierarchical Schur complement elimination procedure that involves computing inverses of small and well-conditioned matrices. When all the unknowns corresponding to inner subdomains interfaces have been eliminated, we reduce the original linear system of equations to a much smaller one involving unknowns on the inner and outer artificial boundary. Basically, if $\mathcal{O}(N)$ unknowns are needed for the solution of the global multiple scattering problem, our final stage linear system requires only $\mathcal{O}(N^{1/2})$ unknowns. The matrix corresponding to this linear system has a block-sparse structure, the distributions of the populated blocks in the global matrix corresponding to the interconnectivity between the subdomains. Harkening back to ideas pertaining to nested dissection methods [14] and multifrontal methods [9] for the solution of sparse linear algebra problems related to finite difference/finite element discretizations, we solve the ensuing linear system by Gaussian elimination of the unknowns corresponding to inner interfaces between subdomains via Schur complements.

The Schur complement elimination procedure that is central to our algorithm is equivalent to a hierarchical merging of the subdomains Robin-to-Robin maps to compute the global interior Robin-to-Robin map of the domain that contains inside the cloud of scatterers. The ideas of using Schur complements for solution of DDM for wave propagation problems was presented in [4] in the context of scattering by deep cavities. The same idea was used in [16] for the solution of scattering problems in variable media, where subdomain spectral solvers are merged via Robin-to-Robin maps. This idea harkens back to the multidomain spectral solvers introduced in [26, 19, 27]. Similar ideas were used recently for multiple scattering problems [23] by random arrays of circular scatterers where the authors merge subdomain (slabs in their case) solutions via Dirichlet-to-Neumann operators. The authors in [23] refer to their algorithm as slab-clustering technique, and solve each slab (subdomain) problems with addition theorem multipole techniques for circular scatterers. Another application of DD Schur complement techniques can be found in computing in a stable manner the impedance of layered elastic media [25].

In the final stage of our algorithm, we solve directly a linear system that involves interior and exterior Robin-to-Robin maps on the boundary of the domain that encloses the ensemble of scatterers. This last inversion turns out to be the dominant contributor to the computational cost of our algorithm: if $\mathcal{O}(N)$ discretization points are needed on the scatterers, the cost of our Schur complement DD algorithm is $\mathcal{O}(N^{3/2})$. More importantly, since we essentially construct a direct solver for multiple scattering problems, multiple incidences can be treated with virtually no additional overhead.

We present later a robust boundary integral operators based representation of the Robin-to-Robin maps that uses the regularization ideas developed in [6, 1]. We will show that the polynomially graded mesh Nyström method introduced in [1, 8, 28] for discretization of Helmholtz boundary integral operators in Lipschitz domains

leads to efficient calculations via direct solvers of subdomain Robin-to-Robin maps for two-dimensional multiple scattering problems.

We will present numerical evidence that our Schur complement DD algorithm gives rise to important computational savings over direct methods for the solution of multiple scattering problems. The solutions of each of these subproblems are interconnected via boundary conditions that reflect properties of the solution of the original problem. The latter solution is typically retrieved through a fixed-point iterative procedure from the subproblem solutions [7, 24]. However, the rate of convergence of the fixed-point iterations is very slow [5]. In order to accelerate the speed of convergence of iterative DD algorithms, carefully designed transmission operators have been incorporated in the Robin data [12, 5].

3.3 The Mathematical Formalization of Domain Decomposition

For the sake of brevity, the details that follow will focus on the case of two scatterers, noting that the general case of larger collections can be treated similarly by sequentially repeating the procedure for adjacent subdomains, although we will advise for an optimal order of mergers towards the end of this chapter that will result in the lowest possible computational cost.

In terms of creating the artificial interface (i.e., the partitioning of the domain), the simplest geometry we can think of is a collection of non-overlapping boxes (rectangular regions) that are connected so as to produce a bigger box that encloses the whole collection of scatterers. Similarly, one could work in polar or spherical to embed a growing collection of circles so that subproblems are solved in each annulus. There are surely cases where the geometry of a given problem would not easily allow for partitioning but for the purposes of multiple acoustic scattering, we will suppose that the scatterers are well separated and the geometry of the subdomains resulting from partitioning is easily trackable in terms of parametrization. See below for the simplest case of two soft-sound scatterers.

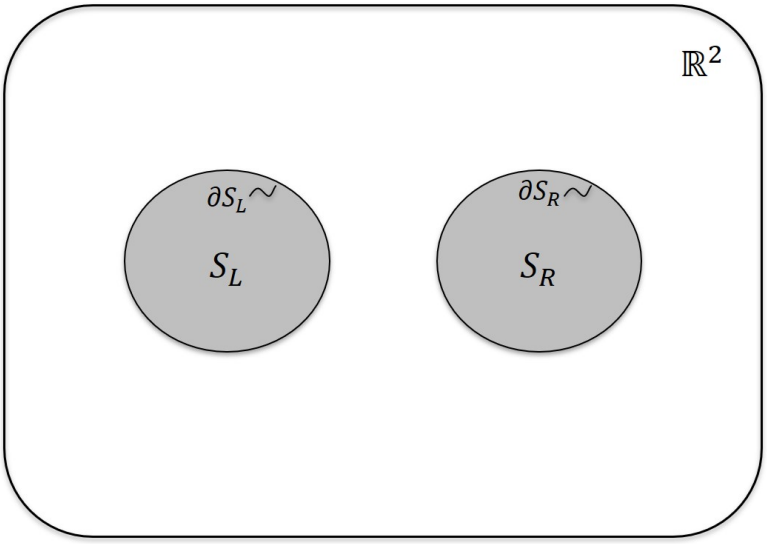

Figure 3.3 Two scatterers in the plane.

The corresponding problem should be well known by now: Find the acoustic field u^s that results as an incident plane wave $u^{inc}(\mathbf{x}) = e^{ik\mathbf{x}\cdot\mathbf{d}}$ travelling in direction $\mathbf{d}$ with wavenumber k impinges upon the boundary $\Gamma := \partial S$ of an impenetrable multiple scatterer $S = S_L \cup S_R$, so that any wave propagation occurs in the exterior of S:

$$\Delta u^s + k^2 u^s = 0 \text{ in } \Omega := \mathbb{R}^2 \backslash S_L \cup S_R,$$

$$u^s = -u^{inc} \text{ on } \Gamma,$$

$$\lim_{r\to\infty} r^{\frac{1}{2}} \left(\frac{\partial u^s}{\partial r} - iku^s \right) = 0, \quad r = |\mathbf{x}|.$$

We split the unbounded domain by enclosing the two scatterers in two adjacent box shaped domains B_L, B_R with respective boundaries ∂B_L and ∂B_R that have an edge in common—see below. It should be stressed that these boxes are purely artificial and do not alter the nature of the problem. Next, let us introduce the following notations which can also be read from the graphical aid provided below:

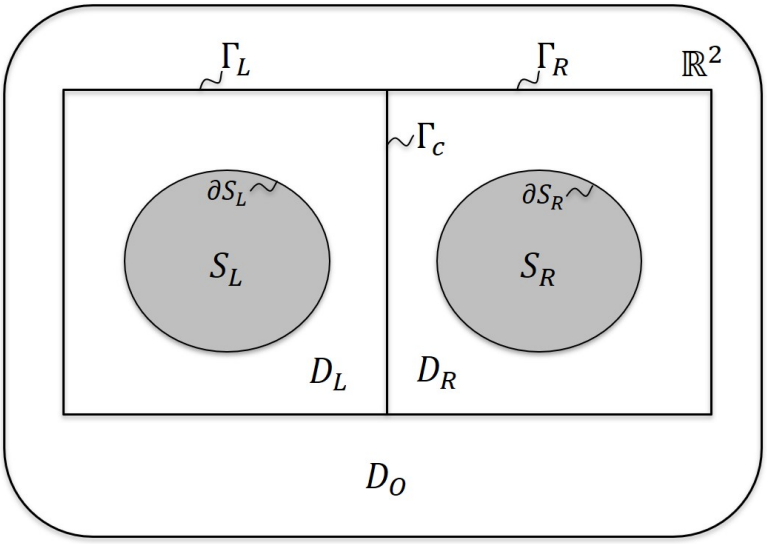

Figure 3.4 Partition of the plane into three subdomains.

Notations

- $D_L := B_L \backslash \overline{S_L}$ :: Left Interior Subdomain
- $D_R := B_R \backslash \overline{S_R}$ :: Right Interior Subdomain
- $D_O := \mathbb{R}^2 \backslash \overline{B_L \cup B_R}$ :: Exterior Subdomain
- $\Gamma_C := \partial B_L \cap \partial B_R$ :: Shared innterface between D_L and D_R
- $\Gamma_L := \partial B_L \backslash \Gamma_C$ :: Shared interface between D_L and D_O
- $\Gamma_R := \partial B_R \backslash \Gamma_C$ :: Shared interface between D_R and D_O
- $\Gamma_O := \Gamma_L \cup \Gamma_R$ :: Boundary of the exterior subdomain D_O

For each subdomain $D_j, j \in \{L, R, O\}$, we denote by $\mathbf{n}_j$ the outward pointing unit normal and by u^j the solution to the Helmholtz equation in that domain. Given that we introduce boundaries not present in the original multiple scattering problem, we have to define new boundary conditions on these. Following the approach introduced by P.L. Lions for elliptic problems and by B. Despres for the Helmholtz problems, we enforce the continuity of Robin data across the interfaces Γ_C, Γ_L and Γ_R. More specifically, the DDM consist of the following suite of coupled Helmholtz problems:

Left Subproblem

$$
\begin{aligned}
\Delta u^L + k^2 u^L &= 0 \text{ in } D_L \\
u^L &= 0 \text{ on } \partial S_L \\
\partial_{n_L} u^L - iku^L &= -\left(\partial_{n_R} u^R + iku^R\right) \text{ on } \Gamma_C \\
\partial_{n_L} u^L - iku^L &= -\left(\partial_{n_O} u^O + iku^O\right) - \partial_{n_O} u^{inc} - iku^{inc} \text{ on } \Gamma_L
\end{aligned}
$$

Right Subproblem

$$
\begin{aligned}
\Delta u^R + k^2 u^R &= 0 \text{ in } D_R \\
u^R &= 0 \text{ on } \partial S_R \\
\partial_{n_R} u^R - iku^R &= -\left(\partial_{n_L} u^L + iku^L\right) \text{ on } \Gamma_C \\
\partial_{n_R} u^R - iku^R &= -\left(\partial_{n_O} u^O + iku^O\right) - \partial_{n_O} u^{inc} - iku^{inc} \text{ on } \Gamma_R
\end{aligned}
$$

Exterior Subproblem

$$
\begin{aligned}
\Delta u^O + k^2 u^O &= 0 \text{ in } D_O \\
\partial_{n_O} u^O - iku^O &= -\left(\partial_{n_L} u^L + iku^L\right) - \partial_{n_O} u^{inc} + iku^{inc} \text{ on } \Gamma_L \\
\partial_{n_O} u^O - iku^O &= -\left(\partial_{n_R} u^R + iku^R\right) - \partial_{n_O} u^{inc} + iku^{inc} \text{ on } \Gamma_R \\
\lim_{r\to\infty} r^{\frac{1}{2}} &\left(\frac{\partial u^O}{\partial r} - iku^O\right) = 0
\end{aligned}
$$

DDM solve for unknowns that are the outgoing Robin boundary data $g^j := (\partial_n u^j - iku^j)|_{\Gamma_j}$ for $j \in \{L, R, O\}$. Clearly the Robin data features explicitly on the left-hand side of each subproblem's statement. The dependence of the righ-hand side expressions on the aforementioned Robin data can be expressed via the so-called Robin-to-Robin (RtR) boundary operators $\mathcal{S}^j g^j := (\partial_n u^j + iku^j)|_{\Gamma_j \cup \Gamma_C}$,

which acts as a correspondence between incoming and outgoing data and where we may interchangeably refer to interior($j = L, R$) and exterior ($j = O$) maps. For $j \in \{L, R\}$, we also make use of a pair of Robin-to-Neumann (RtN) maps $\mathcal{T}^j g^j := \partial_n u^j|_{\partial S_j}$ that link the Robin data on a subdomain to the Neumann data on the scatterer included in that subdomain. All the details regarding the computation of these maps can be found in Chapter 4.

We further split the Robin data $g_j, j \in \{L, R, O\}$ according to subdomain interfaces and we effect similar splittings of the RtR and RtN maps:

- $\mathcal{S}^L g^L =: \begin{bmatrix} \mathcal{S}^L_{ll} & \mathcal{S}^L_{cl} \\ \mathcal{S}^L_{lc} & \mathcal{S}^L_{cc} \end{bmatrix} \begin{bmatrix} g^L_l \\ g^L_c \end{bmatrix} = \begin{bmatrix} (\partial_n u^L + iku^L)|_{\Gamma_L} \\ (\partial_n u^L + iku^L)|_{\Gamma_C} \end{bmatrix}$
- $\mathcal{S}^R g^R =: \begin{bmatrix} \mathcal{S}^R_{rr} & \mathcal{S}^R_{cr} \\ \mathcal{S}^R_{rc} & \mathcal{S}^R_{cc} \end{bmatrix} \begin{bmatrix} g^R_r \\ g^R_c \end{bmatrix} = \begin{bmatrix} (\partial_n u^R + iku^R)|_{\Gamma_R} \\ (\partial_n u^R + iku^R)|_{\Gamma_C} \end{bmatrix}$
- $\mathcal{S}^O g^O =: \begin{bmatrix} \mathcal{S}^O_{ll} & \mathcal{S}^O_{rl} \\ \mathcal{S}^O_{lr} & \mathcal{S}^O_{rr} \end{bmatrix} \begin{bmatrix} g^O_l \\ g^O_r \end{bmatrix} = \begin{bmatrix} (\partial_n u^O + iku^O)|_{\Gamma_L} \\ (\partial_n u^O + iku^O)|_{\Gamma_R} \end{bmatrix}$
- $\mathcal{T}^L g^L =: \begin{bmatrix} \mathcal{T}^L_l & \mathcal{T}^L_c \end{bmatrix} \begin{bmatrix} g^L_l \\ g^L_c \end{bmatrix} = \partial_n u^L|_{\partial S_L}$
- $\mathcal{T}^R g^R =: \begin{bmatrix} \mathcal{T}^R_r & \mathcal{T}^R_c \end{bmatrix} \begin{bmatrix} g^R_r \\ g^R_c \end{bmatrix} = \partial_n u^R|_{\partial S_R}.$

For the sake of simplicity of notations, the notation **n** in equations above refers to the exterior unit normal to the corresponding subdomain. Assuming that all these maps have been computed, the three part problem above can equivalently

be written in the form of the following linear system:

$$\begin{bmatrix} I & \mathcal{S}_{cc}^R & 0 & \mathcal{S}_{rc}^R & 0 & 0 \\ \mathcal{S}_{cc}^L & I & \mathcal{S}_{lc}^L & 0 & 0 & 0 \\ 0 & 0 & I & 0 & \mathcal{S}_{ll}^O & \mathcal{S}_{rl}^O \\ 0 & 0 & 0 & I & \mathcal{S}_{lr}^O & \mathcal{S}_{rr}^O \\ \mathcal{S}_{cl}^L & 0 & \mathcal{S}_{ll}^L & 0 & I & 0 \\ 0 & \mathcal{S}_{cr}^R & 0 & \mathcal{S}_{rr}^R & 0 & I \end{bmatrix} \begin{bmatrix} g_c^L \\ g_c^R \\ g_l^L \\ g_r^R \\ g_l^O \\ g_r^O \end{bmatrix} = \begin{bmatrix} 0 \\ 0 \\ -(\partial_n u^{inc} + iku^{inc})|_{\Gamma_L} \\ -(\partial_n u^{inc} + iku^{inc})|_{\Gamma_R} \\ -(\partial_n u^{inc} - iku^{inc})|_{\Gamma_L} \\ -(\partial_n u^{inc} - iku^{inc})|_{\Gamma_R} \end{bmatrix} \tag{3.1}$$

or in compact notation:

$$(I + \mathcal{S})g = b.$$

The equivalence of the DDM formulation to the original scattering problems is proved rigorously in our paper [31] using arguments that were borrowed from Collino [15], a key ingredient being the fact that the RtR maps $\mathcal{S}^j$ are isometries. Once having solved for the Robin data g^L, g^R, we compute $\partial_n u^L|_{\partial S_L} = \mathcal{T}^L g^L$ and $\partial_n u^R|_{\partial S_R} = \mathcal{T}^R g^R$ with the help of the RtN maps, from which the scattered field is computed in turn from a simple application of Green's formula:

$$u(\mathbf{x}) = \sum_{j \in \{L,R\}} \int_{\partial S_j} G_k(\mathbf{x} - \mathbf{y}) \partial_{n(\mathbf{y})} u^j(\mathbf{y}) ds(\mathbf{y}), \quad \mathbf{x} \in \Omega.$$

We focus our attention in the sequel to solving efficiently the linear system (3.1). In practice, the size of the DDM linear system can get large, and thus iterative linear algebra methods were historically preferred over direct ones. The most popular iterative solver candidates include the Jacobi (fixed point) method and the GMRES (Krylov Subspace) method. As it turns out, the Jacobi iterative scheme amounts

to:

$$g^{(n+1)} = b - \mathcal{S}g^{(n)}.$$

which is equivalent to find the solution $u^{L,(n+1)}$ of the Helmholtz equation in the domain D_L satisfying the Robin boundary condition:

$$\left(\partial_n u^L - iku^L\right)^{(n+1)} = -\left(\partial_n u^R + iku^R\right)^{(n)} \text{ on } \Gamma_C.$$

We note that subdomains exchange information via Robin boundary conditions in this version of DDM. In this form the DDM is referred to non-overlapping Schwarz iteration. Jacobi iterative methods for Helmholtz DDM methods have been well documented to yield a slow convergence rate due to the fact that the eigenvalues corresponding to high-frequency modes of the matrix $\mathcal{S}$ converge to one. Unfortunately, GMRES solvers do not fare particularly well [15]. This shortcoming can be attributed to the choice of Robin boundary conditions and the outflow/inflow of information from a subdomain to its neighboring subdomains associated with it. Ideally, the subdomain boundary conditions have to be chosen so that information flows out of the subdomain and no information is reflected back into the subdomain. This can be achieved if the term $-ik$ is replaced by the adjacent subdomain Dirichlet to Neumann (DtN) operator restricted to the common interface—in this way the Jacobi scheme converges in precisely two iterations [24]. Since DtN maps are not always well defined and expensive to compute even when properly defined, easily computable approximations of DtN maps can be employed effectively to lead to faster convergence rates of GMRES solvers for DDM algorithms [5]. However, these approximations lead to non-standard boundary conditions and the analysis of the ensuing DDM is hard. To the best of our knowledge, there are no boundary

conditions that work well in practice and at the same time are amenable to rigorous analysis for general subdomains.

The further splitting of Robin data gives rise to sparser matrices whose sparsity pattern resembles that of matrices corresponding to finite differences (more precisely five-point Laplacians). We harken back to ideas from multifrontal methods and nested dissection that amount to an efficient Gaussian elimination through Schur complements of the Ronin unknowns corresponding to the inner interfaces. For example, in the simplified setting of two subdomains, in the first step we eliminate the unknowns g_c^L and g_c^R on the interior interface Γ_C and in the second step we recover the exterior Robin data on Γ_O. Investigating the nature of the matrix resulting after the application of the Schur complement in the first step above we conclude that the first step is essentially a form of algebraic merging of RtR maps corresponding to the interior subdomains. This observation proves particularly useful when dealing with larger subdomain configurations where the first step can simply be applied recursively and hierarchically until all interior unknowns have been eliminated and then the second step is carried out, at the end, only once.

3.3.1 The Merging of Interior Subdomains

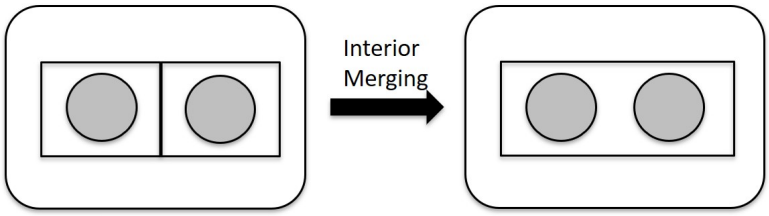

Figure 3.5 Sequential elimination of the interior partition.

Given the matrix in equation (3.1), let us consider only those equations that involve the interior quantities g_c^L and g_c^R. Doing so we get the reduced system corresponding

to the first step of eliminating the data that is shared on the interior skeleton:

$$\begin{bmatrix} I & \mathcal{S}_{cc}^R & 0 & \mathcal{S}_{rc}^R \\ \mathcal{S}_{cc}^L & I & \mathcal{S}_{lc}^L & 0 \\ \mathcal{S}_{cl}^L & 0 & \mathcal{S}_{ll}^L & 0 \\ 0 & \mathcal{S}_{cr}^R & 0 & \mathcal{S}_{rr}^R \end{bmatrix} \begin{bmatrix} g_c^L \\ g_c^R \\ g_l^L \\ g_r^R \end{bmatrix} = \begin{bmatrix} 0 \\ 0 \\ -(\partial_n u^{inc} - iku^{inc})|_{\Gamma_L} - g_l^O \\ -(\partial_n u^{inc} - iku^{inc})|_{\Gamma_R} - g_r^O \end{bmatrix} = \begin{bmatrix} 0 \\ 0 \\ (\partial_n u^L + iku^L)|_{\Gamma_L} \\ (\partial_n u^R + iku^R)|_{\Gamma_R} \end{bmatrix}$$

where we used $-(\partial_n u^{inc} - iku^{inc})|_{\Gamma_j} - g_j^O = (\partial_n u^j + iku^j)|_{\Gamma_j}$ for $j = L, R$. Equivalently, the last equation can be written in block notation in the following form:

$$\begin{bmatrix} A & B \\ C & D \end{bmatrix} \begin{bmatrix} g^C \\ g^{L\cup R} \end{bmatrix} = \begin{bmatrix} 0 \\ (\partial_n u^{L\cup R} + iku^{L\cup R})|_{\Gamma_O} \end{bmatrix},$$

where we defined:

$$A := \begin{bmatrix} I & \mathcal{S}_{cc}^R \\ \mathcal{S}_{cc}^L & I \end{bmatrix}, \quad B := \begin{bmatrix} 0 & \mathcal{S}_{rc}^R \\ \mathcal{S}_{lc}^L & 0 \end{bmatrix}, \quad C := \begin{bmatrix} \mathcal{S}_{cl}^L & 0 \\ 0 & \mathcal{S}_{cr}^R \end{bmatrix}, \quad D := \begin{bmatrix} \mathcal{S}_{ll}^L & 0 \\ 0 & \mathcal{S}_{rr}^R \end{bmatrix},$$

and

$$g^C := \begin{bmatrix} g_c^L \\ g_c^R \end{bmatrix}, \quad g^{L\cup R} := \begin{bmatrix} g_l^L \\ g_r^R \end{bmatrix}.$$

Our goal in this first step is to eliminate the interior data g^C. From $Ag^C + Bg^{L\cup R} = 0$ we have that $g^C = -A^{-1}Bg^{L\cup R}$ and upon substitution in the second equation we derive the following equation:

$$(D - CA^{-1}B)g^{L\cup R} = (\partial_n u^{L\cup R} + iku^{L\cup R})|_{\Gamma_O}. \tag{3.2}$$

Denoting:

$$M := \begin{bmatrix} A & B \\ C & D \end{bmatrix},$$

we recognize on the left-hand side of the equation above the familiar Schur complement $M/A = D - CA^{-1}B$, and on the right-hand side the expression $(\partial_n u^{L\cup R} + iku^{L\cup R})|_{\Gamma_O}$. The insight in the equation above is that it relates two quantities in a manner reminiscent of RtR operators:

$$g^{L\cup R} \xrightarrow{M/A} (\partial_n u^{L\cup R} + iku^{L\cup R})|_{\Gamma_O}. \tag{3.3}$$

The map in equations (3.2) and (3.3) is an effective means to merge two RtR operators $\mathcal{S}^L$ and $\mathcal{S}^L$ acting on the boundaries of two adjacent boxes B_L and B_R, respectively, to form the RtR operator $\mathcal{S}^{L\cup R}$ of the merged box $B_L \cup B_R$. The latter operator maps the Robin data $g^{L\cup R} = (\partial_n u^{L\cup R} - iku^{L\cup R})|_{\Gamma_O}$ related to a solution $u^{L\cup R}$ of the Helmholtz equation in the domain $B_L \cup B_R$ with zero Dirichlet boundary conditions on ∂S_L and ∂S_R to the corresponding quantity $(\partial_n u^{L\cup R} + iku^{L\cup R})|_{\Gamma_O}$. The merging procedure can be easily extended to produce the merged RtN map for the domain $B_L \cup B_R$. Indeed, recall the definition of subdomain RtN maps:

$$\mathcal{T}^L g^L =: \begin{bmatrix} \mathcal{T}_l^L & \mathcal{T}_c^L \end{bmatrix} \begin{bmatrix} g_l^L \\ g_c^L \end{bmatrix} = \partial_n u^L|_{\partial S_L}, \quad \mathcal{T}^R g^R =: \begin{bmatrix} \mathcal{T}_r^R & \mathcal{T}_c^R \end{bmatrix} \begin{bmatrix} g_r^R \\ g_c^R \end{bmatrix} = \partial_n u^R|_{\partial S_R}.$$

Denoting:

$$\mathcal{C} := \begin{bmatrix} \mathcal{T}_c^L & 0 \\ 0 & \mathcal{T}_c^R \end{bmatrix}, \quad \mathcal{D} := \begin{bmatrix} \mathcal{T}_l^L & 0 \\ 0 & \mathcal{T}_r^R \end{bmatrix}, \quad \text{and } \partial_n u^{L\cup R}|_{\partial S_L \cup \partial S_R} := \begin{bmatrix} \partial_n u^L|_{\partial S_L} \\ \partial_n u^R|_{\partial S_R} \end{bmatrix}$$

we can write the two RtN maps compactly as:

$$\mathcal{C}g^C + \mathcal{D}g^{L\cup R} = \partial_n u^{L\cup R}|_{\partial S_L \cup \partial S_R}. \tag{3.4}$$

Upon replacing the previously derived expression $g^C = -A^{-1}B$ in equation (3.4) we obtain the merged RtN map we were looking for:

$$(\mathcal{D} - \mathcal{C}A^{-1}B)g^{L\cup R} = \partial_n u^{L\cup R}|_{\partial S_L \cup \partial S_R}. \tag{3.5}$$

We note that computing the merged RtN map according to formula (3.5) requires little additional computational cost, as we already computed A^{-1} in the RtR merging procedure. Accordingly, the merging of interior RtR and RtN maps can be performed simultaneously. Another natural question arises: when is it more advantageous to compute the RtR map of the domain $B_L \cup B_R$ through algebraic merging of subdomain RtR maps rather than directly?

Given that the RtR maps encode information about all of the scatterers included in each subdomain, it would appear natural that the merging approach could be more profitable when there is a large number of scatterers included in each subdomain. To encapsulate all the work done to this point and to further emphasize that the merging happens simultaneously, we have the following theorem.

Theorem 2. *Given a pair of boundary operators:*

$$\begin{bmatrix} \mathcal{S}^L \\ \mathcal{T}^L \end{bmatrix} : L^2(\partial B_L) \to L^2(\partial B_L) \times L^2(\partial S_L),$$

$$g^L \mapsto \begin{bmatrix} (\partial_n u^L + iku^L)|_{\partial B_L} \\ (\partial_n u^L)|_{\partial S_L} \end{bmatrix},$$

and

$$\begin{bmatrix} \mathcal{S}^R \\ \mathcal{T}^R \end{bmatrix} : L^2(\partial B_R) \to L^2(\partial B_R) \times L^2(\partial S_R),$$

$$g^R \mapsto \begin{bmatrix} (\partial_n u^R + iku^R)|_{\partial B_R} \\ (\partial_n u^R)|_{\partial S_R} \end{bmatrix},$$

defined on two adjacent boxes B_L and B_R, there exists a unique merged map:

$$\begin{bmatrix} \mathcal{S}^{L\cup R} \\ \mathcal{T}^{L\cup R} \end{bmatrix} : L^2(\Gamma_O) \to L^2(\Gamma_O) \times L^2(\partial S_L \cup \partial S_R),$$

$$g^{L\cup R} \mapsto \begin{bmatrix} (\partial_n u^{L\cup R} + iku^{L\cup R})|_{\Gamma_O} \\ (\partial_n u^{L\cup R})|_{\partial S_L \cup \partial S_R} \end{bmatrix},$$

given by:

$$\begin{bmatrix} \mathcal{S}^{L\cup R} \\ \mathcal{T}^{L\cup R} \end{bmatrix} = \begin{bmatrix} D \\ \mathcal{D} \end{bmatrix} - \begin{bmatrix} C \\ \mathcal{C} \end{bmatrix} A^{-1} B,$$

where $A, B, C, D, \mathcal{C}, \mathcal{D}$ are all recounted above.

As a corollary, if we carry out the algebra from the last theorem, we get explicit representation of the aforementioned operators:

Corollary

$$\mathcal{S}^{L\cup R} = D - CA^{-1}B = \begin{bmatrix} \mathcal{S}^L_{ll} - \mathcal{S}^L_{cl}W^{-1}\mathcal{S}^R_{cc}\mathcal{S}^L_{lc} & \mathcal{S}^L_{cl}W^{-1}\mathcal{S}^R_{rc} \\ \\ \mathcal{S}^R_{cr}(\mathcal{S}^L_{cc}W^{-1}\mathcal{S}^R_{cc} - I)\mathcal{S}^L_{lc} & \mathcal{S}^R_{rr} - \mathcal{S}^R_{cr}\mathcal{S}^L_{cc}W^{-1}\mathcal{S}^R_{rc} \end{bmatrix},$$

and

$$\mathcal{T}^{L\cup R} = \mathcal{D} - \mathcal{C}A^{-1}B = \begin{bmatrix} \mathcal{T}^L_{l} - \mathcal{T}^L_{c}W^{-1}\mathcal{S}^R_{cc}\mathcal{S}^L_{lc} & \mathcal{T}^L_{c}W^{-1}\mathcal{S}^R_{rc} \\ \\ \mathcal{T}^R_{c}(\mathcal{S}^L_{cc}W^{-1}\mathcal{S}^R_{cc} - I)\mathcal{S}^L_{lc} & \mathcal{T}^R_{r} - \mathcal{T}^R_{c}\mathcal{S}^L_{cc}W^{-1}\mathcal{S}^R_{rc} \end{bmatrix},$$

where $W = \mathcal{S}^R_{cc}\mathcal{S}^L_{cc} - I$ represents the only quantity that needs to be inverted during the merging procedure.

To conclude this section, we remind that the general treatment of bigger configurations is easily achieved by repeating the process. Indeed, one could simply apply in a sequential fashion the merging of two adjacent subdomains over and over again until the whole interior partition has been eliminated. However, some care is advised as a naive approach to performing the interior merging can easily lead to a sub optimal performance. While partitions that consist only of a single row or column of subdomains do not allow for any choice of sequence in the merging strategy, we advise to choose the sequence in the remaining cases so as to minimize the overall number of large mergings that occur towards the last steps. To motivate the idea, let's consider an example in which we assume for

convenience that a box domain B is to be partitioned into a collection of smaller boxes $\{B_{ij}\}, i = 1, ..., 2^k, j = 1, ..., 2^l$. Figure 3.6 below exposes a case in which the chosen merging sequence is not optimal, since the CPU is being taxed with the biggest matrix inversion not only in the last step, but two other times in previous step, for a total of three times.

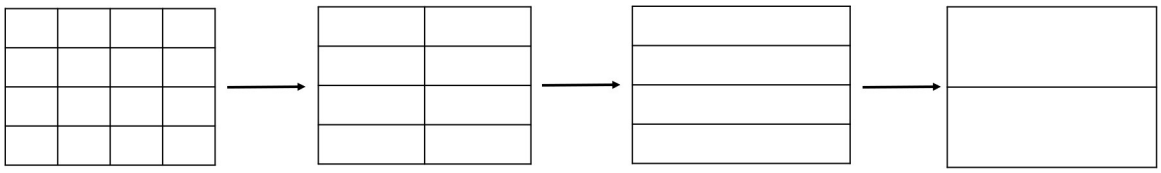

Figure 3.6 Sub optimal merging sequence.

The optimal strategy for domains whose edges are powers of 2 in both directions is to proceed in a *quadtree* fashion so that at every other step the partitioning preserves square subdomains. This strategy is done by alternating between left-right and up-down mergings between steps as shown in Figure 3.7. The procedure goes on for as long as both $i > 1$ and $j > 1$. When either $i = 1$ or $j = 1$, one is left with a strip of subdomains that no longer requires a choice of merging order, unless perhaps when the subdomains are identical then it is still advisable to preserve the configuration of subdomains as powers of two since at each step only one map needs to be computed. The same obviously goes for the whole procedure - if the whole domain was divided into a collection of identical subdomains, then a lot of effort can be saved by computing the augmented RtR map only once per step.

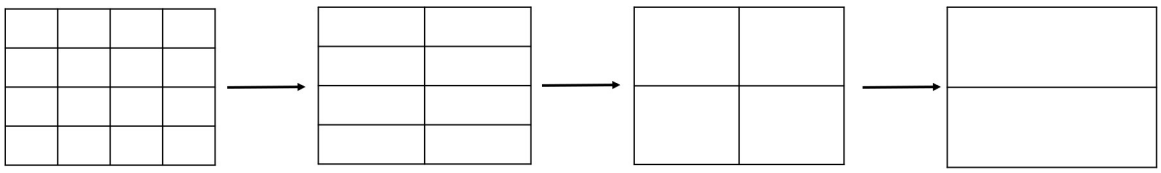

Figure 3.7 Quadtree optimal merging sequence.

3.3.2 The Merging of Interior and Exterior Subdomains

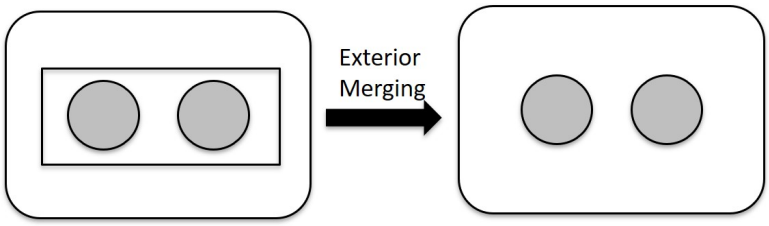

Figure 3.8 Interior-exterior merging.

If we go back to the linear system (3.1) after eliminating the interior unknown quantities g_c^L and g_c^R, we obtain a reduced system only in terms of maps defined on Γ_O:

$$\begin{bmatrix} I & \mathcal{S}^O \\ \mathcal{S}^{L\cup R} & I \end{bmatrix} \begin{bmatrix} g^{L\cup R} \\ g^O \end{bmatrix} = \begin{bmatrix} -(\partial_n u^{inc} + iku^{inc})|_{\Gamma_O} \\ -(\partial_n u^{inc} - iku^{inc})|_{\Gamma_O} \end{bmatrix}.$$

As pointed out earlier, the merging procedure yields a map $\mathcal{S}^{L\cup R}$ that is equivalent to one that we would get should we compute it directly without any interior partitioning. This system, therefore, shows an alternative method for solving the Helmholtz problem with a two subdomains partition, namely exterior and interior. This of course is only of theoretical interest, since the numerical cost of computing an interior map is always greater than solving the boundary integral equation on the scatterers within its underlying box. Nonetheless, this is not just a mere observation as it reinforces the importance of being able to compute the final interior map as efficiently as possible. It should also be clear from this that the bigger the problem (in terms of number of scatterers), the more competitive the method will prove to be when compared with a classical solver that does not take advantage of domain partitioning.

Going back to the reduced system, since both g^O and $g^{L\cup R}$ involve the same quantities, it suffices to solve for g^O alone, which gives:

$$g^O = (I - \mathcal{S}^{L\cup R}\mathcal{S}^O)^{-1}\left(\mathcal{S}^{L\cup R}(\partial_n u^{inc} + iku^{inc})|_{\Gamma_O} - (\partial_n u^{inc} - iku^{inc})|_{\Gamma_O}\right).$$

The Dirichlet and Neumann data is then easily recovered from linear combinations of:

$$\begin{aligned}\partial_n u^s|_{\Gamma_O} - iku^s|_{\Gamma_O} =& g^O,\\ \partial_n u^s|_{\Gamma_O} + iku^s|_{\Gamma_O} =& \mathcal{S}^O g^O,\end{aligned}$$

and give:

$$\begin{aligned}u^s|_{\Gamma_O} =& \frac{1}{2}(\mathcal{S}^O - I)g^O,\\ \partial_n u^s|_{\Gamma_O} =& \frac{1}{2}(\mathcal{S}^O + I)g^O.\end{aligned}$$

It is important to note that for the purpose of exterior computations alone, one could stop there and use a Green's representation on Γ_O with $u^s|_{\Gamma_O}$ and $\partial_n u^s|_{\Gamma_O}$. For a solution everywhere, one would need to append the extra step:

$$\partial_n(u^s + u^{inc})|_{\partial S_L\cup\partial S_R} = -\mathcal{T}^{L\cup R}\left(\partial_n(u^s + u^{inc}) + ik(u^s + u^{inc})\right)|_{\Gamma_O},$$

where the minus sign is to account for the fact that the solution is given in terms of exterior quantities (g^O) and $\mathcal{T}$ is an interior map, so the normal $\mathbf{n}$ needs to be inverted.

3.4 The Cost Analysis of Domain Decomposition

If you followed the discussion closely up until this point, you may have noticed that the cost of the merging procedure is dominated by that of solving for the unknowns pertaining to the exterior boundary Γ_O.

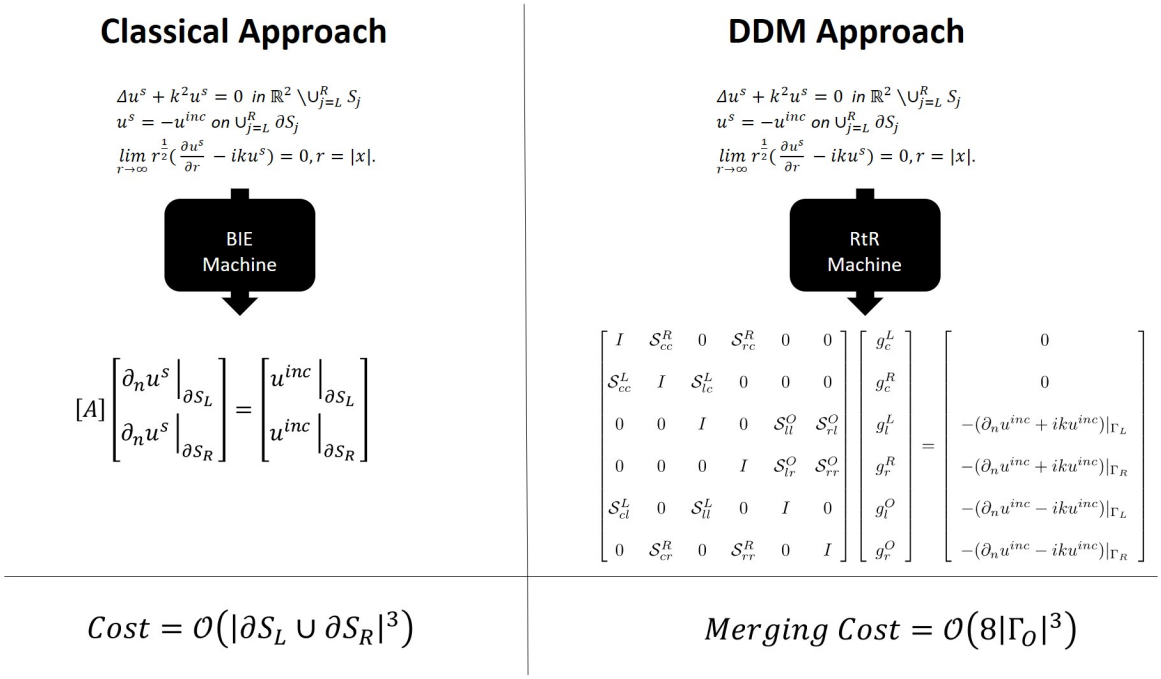

Figure 3.9 Direct vs DDM costs.

If the objective is to design a more efficient algorithm than the direct solver, we need to find a way to relate the choice of discretization of $\cup_i \partial S_i$ to the choice of discretization of Γ_O so that we can readily compare $|\cup_i \partial S_i|$ and $|\Gamma|$. Let us argue with the help of an example to motivate the relationship that we seek. Consider the following choices of configurations, all representing a single box domain enclosing a collection of arc segments.

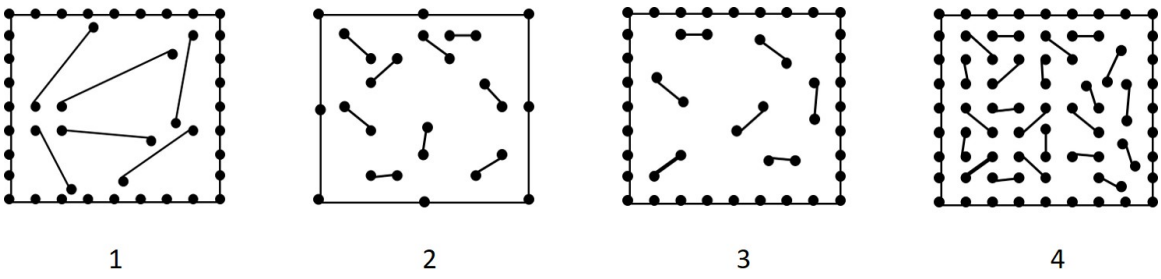

Figure 3.10 Different choices of discretizations.

We note that in the first two cases the choice of precision on the box is inconsistent with the one chosen on the scatterers. This is problematic for either one or the other following reasons. In the first case, we observe that a coarse mesh is used on the scatterers, (which ought to be dictated by the wave number) and a finer one is used on the box. This is a scenario where one is wasting resources by computing the RtR map with more points than it is actually needed because these maps do not add information to the given problem.

The second case is the opposite scenario where a fine mesh is employed on the scatterer, but all that precision is then lost once encoded by the map who does not use enough points on the box. In essence, what we want here is to be able to encode all the information for as cheaply as possible without loosing any precision. This is achieved by ensuring that the amount of points per wavelength used on the scatterers and the box be roughly the same.

Finally, we note that in the last two presented choices, the mesh precision on the scatterers and the box is consistent, but the last case is seen to encode a lot more information because most of its interior is occupied while the third case has a lot of empty space in its interior and so does not seem to take full advantage of the method.

When one opts to enclose as many scatterers as possible such as in the fourth case, then we see from the picture that the limiting relationship is to allocate $\sqrt{n}$ on each side of the box whenever n points densely occupy its interior.

For a general domain decomposed into a collection of $l_1 \times l_2$ subdomains, each containing n points in their inside, the cost of merging is dominated by $\mathcal{O}((4(l_1 + l_2)\sqrt{n})^3)$, and for square configurations, $(l_1 = l_2 = l)$, this becomes $\mathcal{O}((8l\sqrt{n})^3)$.

In order to get the total cost of the DD procedure, one also has to account for the cost of obtaining the individual maps in the first place. A quick overview of the next chapter reveals that this cost is $\mathcal{O}(l^2(n + 4\sqrt{n})^3) = \mathcal{O}(l^2 n^3)$. We encapsulate these results in the following:

Result: The total cost of the DDM procedure for a square domain decomposed into a collection of $l \times l$ square subdomains, each enclosing a uniform and dense distribution of n collocation points in their interior is :

$$\mathcal{O}(l^2 n^3) + \mathcal{O}((8l\sqrt{n})^3).$$

By comparison, the direct cost of solving this configuration of $N := l^2 n$ points is $\mathcal{O}(l^6 n^3)$, hence the optimal strategy is to choose a partition that maximizes l and minimizes n.

We close this chapter with the results of an experiment that was carried out for a box configuration containing a total of $10,240$ collocation points in its interior for different choices of partitioning. As expected, the reported times (in seconds) are best for smaller subdomains.

			Time	DDM Times			
N	l	n	Direct BIE	Maps	Interior Merging	Exterior Merging	Total
			$\mathcal{O}(l^6 n^3)$	$\mathcal{O}(l^2 n^3)$	$\mathcal{O}((l\sqrt{n})^3)$	$\mathcal{O}((8l\sqrt{n})^3)$	
10240	16	40	**63.47**	1.84	0.40	0.24	**2.49**
10240	8	160	**67.93**	2.00	0.28	0.24	**2.52**
10240	4	640	**66.92**	4.83	0.13	0.23	**5.18**
10240	2	2560	**67.57**	13.43	0.07	0.25	**13.76**
10240	1	10240	**71.81**	84.70	N/A	0.27	**84.97**

Figure 3.11 Time comparisons of DDM vs direct approach.

CHAPTER 4

CONSTRUCTION OF THE RTR AND RTN BOUNDARY OPERATORS

4.1 The Interior Robin-to-Robin and Robin-to-Neumann Operators

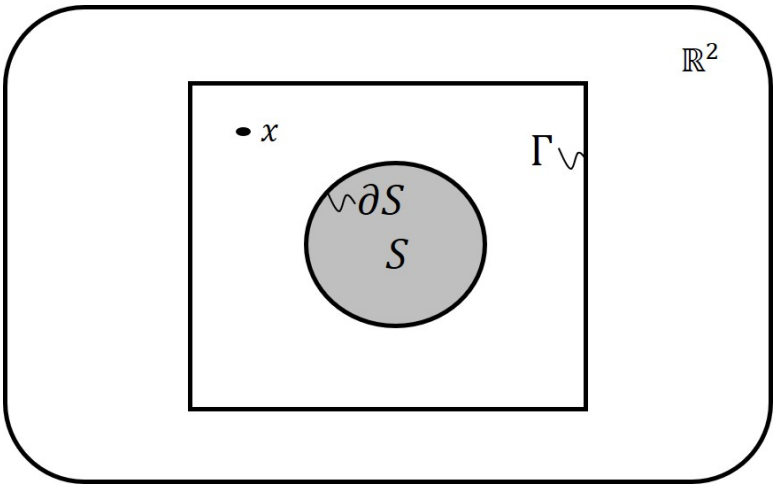

Figure 4.1 The setting for computing the interior map.

In this section, we go over the details of computing the RtR and RtN maps. In order to keep the notations simple, we consider the case of one closed Lipschitz scatterer S inside of a box subdomain B and the following Helmholtz boundary value problem:

$$\begin{aligned} \Delta u + k^2 u = &\quad 0, \qquad \text{in } B \setminus S, \\ u = &\quad 0, \qquad \text{on } \partial S, \\ \partial_n u + z u = &\quad g^{int}, \qquad \text{on } \Gamma := \partial B, \end{aligned} \tag{4.1}$$

where the wavenumber k is assumed to be positive, g^{int} is the data defined on Γ, and $z = i\eta, \eta \in \mathbb{R}$ is an impedance coefficient. In equation (4.1), the normal derivative is taken with respect to the unit normal pointing outside of the domain B. We recall

that the RtR map for this configuration was defined as:

$$\mathcal{S}^{Int}(\partial_n u + zu)|_\Gamma = \partial_n u|_\Gamma - zu|_\Gamma.$$

Since $\partial_n u|_\Gamma - zu|_\Gamma = g^{int} - 2zu|_\Gamma$, we can alternatively write:

$$\mathcal{S}^{Int} g^{int} = g^{int} - 2zu|_\Gamma.$$

Hence, we observe that if we can find a Robin-to-Dirichlet operator $\mathcal{A}_\Gamma$ that satisfies $u|_\Gamma = \mathcal{A}_\Gamma g^{int}$, then we could conclude that $\mathcal{S}^{Int} = I_\Gamma - 2z\mathcal{A}_\Gamma$. The following proposition settles the question of obtaining $\mathcal{S}^{Int}$ by showing how to jointly compute the Robin-to-Dirichlet and the Robin-to-Neumann maps.

Theorem 3. *The pair of interior RtR and RtN boundary operators $\mathcal{S}^{Int}$ and $\mathcal{T}$ are jointly obtained through:*

$$\begin{aligned}\mathcal{S}^{Int} =& I_\Gamma - 2z\ \mathcal{A}_\Gamma,\\ \mathcal{T} =& \mathcal{A}_{\Gamma,\partial S},\end{aligned}$$

where:

$$\mathcal{A} := \begin{bmatrix} \mathcal{A}_\Gamma \\ \mathcal{A}_{\Gamma,\partial S} \end{bmatrix} = \begin{bmatrix} \left[\frac{1}{2}I + zV + K\right]_\Gamma & SL_{\partial S,\Gamma} \\ [zSL + DL]_{\Gamma,\partial S} & V_\Gamma \end{bmatrix}^{-1} \begin{bmatrix} V_\Gamma \\ SL_{\Gamma,\partial S} \end{bmatrix}.$$

Proof. From $g^{int} := (\partial_n u + zu)|_\Gamma$ we see that $\partial_n u|_\Gamma = g^{int} - zu|_\Gamma$ and from Green's representation of the solution in the domain $B \setminus S$:

$$u(\mathbf{x}) = \left[SL_\Gamma \partial_n u|_\Gamma - DL_\Gamma u|_\Gamma - SL_{\partial S} \partial_n u|_{\partial S}\right](\mathbf{x}), \quad \mathbf{x} \in B \setminus S,$$

then taking the limit as $\mathbf{x} \to \Gamma^-$, we obtain a first set of equations (we drop the $\mathbf{x}$ dependence)

$$\begin{aligned} u|_\Gamma &= V_\Gamma \partial_n u|_\Gamma - K_\Gamma u|_\Gamma + \frac{1}{2} u|_\Gamma - SL_{\partial S,\Gamma} \partial_n u|_{\partial S}, \\ &\leftrightarrow \\ \frac{1}{2} u|_\Gamma &= V_\Gamma (g^{int} - zu|_\Gamma) - K_\Gamma u|_\Gamma - SL_{\partial S,\Gamma} \partial_n u|_{\partial S}. \end{aligned}$$

Taking the limit as $\mathbf{x} \to \partial S^+$, we obtain a second equation in the form:

$$\begin{aligned} 0 &= SL_{\Gamma,\partial S} \partial_n u|_\Gamma - DL_{\Gamma,\partial S} u|_\Gamma - V_{\partial S} \partial_n u|_{\partial S}, \\ &= SL_{\Gamma,\partial S} (g^{int} - zu|_\Gamma) - DL_{\Gamma,\partial S} u|_\Gamma - V_{\partial S} \partial_n u|_{\partial S}. \end{aligned}$$

Upon reorganizing the equations above in the form of a linear system of equations, we obtain the following:

$$\begin{bmatrix} \left[\frac{1}{2} I + zV + K\right]_\Gamma & SL_{\partial S,\Gamma} \\ \left[zSL + DL\right]_{\Gamma,\partial S} & V_\Gamma \end{bmatrix} \begin{bmatrix} u|_\Gamma \\ \partial_n u|_{\partial S} \end{bmatrix} = \begin{bmatrix} V_\Gamma \\ SL_{\Gamma,\partial S} \end{bmatrix} g^{int},$$

which completes the derivation. □

We remark that the derivations above remain valid in the case when S in an open arc. As one can observe, the calculation of interior RtR and RtN maps requires the inversion of a system of size the number of unknowns on Γ and on ∂S, which

depending on the size of the box can be considerably more demanding than solving directly on a "small" configuration of scatterers included in the box. Hence, both the choice of box size and of partitioning (i.e., the number of scatterers to enclose per box) have to be done with care. While there is no doubt to us that the method is extremely efficient for very large configurations of scatterers (e.g., order of 10,000 scatterers have been performed), we still need to investigate the size requirements for which the DDM is preferable over the direct BIE approach.

Having established how to compute the interior RtR operator $\mathcal{S}^{Int}$, we move on to show in a similar fashion how the exterior map is computed.

4.2 The Exterior Robin-to-Robin Operator

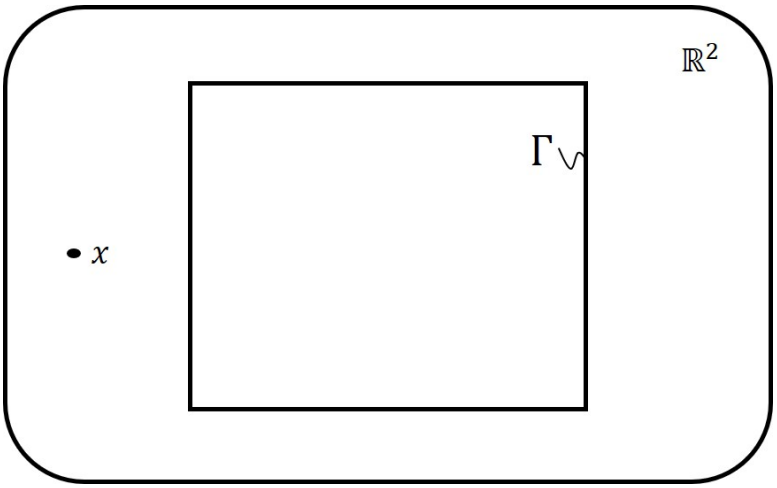

Figure 4.2 The setting for computing the exterior map.

Assume the same setup as before. We want to compute an exterior RtR operator $\mathcal{S}^{Ext}$ that maps the exterior data $g^{ext} := (\partial_n u^s + z u^s)|_\Gamma$ to $(\partial_n u^s - z u^s)|_\Gamma$.

Theorem 4. *The exterior RtR boundary operator $\mathcal{S}^{Ext}$ can be expressed explicitly as:*

$$\mathcal{S}^{Ext} = I_\Gamma - 2z \left(K_\Gamma + zV_\Gamma - \frac{1}{2} I_\Gamma \right)^{-1} V_\Gamma.$$

Proof. As before we will start by expressing the solution with a Green's representation in the exterior of the box B and will make use of $\partial_n u^s|_\Gamma = g^{ext} - z u^s|_\Gamma$.

$$\begin{aligned} u^s(\mathbf{x}) &= \left[DL_\Gamma u^s|_\Gamma - SL_\Gamma \partial_n u^s|_\Gamma \right](\mathbf{x}), \quad \mathbf{x} \in \mathbb{R}^2 \setminus B \\ &= \left[DL_\Gamma u^s|_\Gamma - SL_\Gamma (g^{ext} - z u^s|_\Gamma) \right](\mathbf{x}) \\ &\Big\downarrow \quad \mathbf{x} \to \Gamma^+ \\ & K_\Gamma u^s|_\Gamma + \frac{1}{2} u^s|_\Gamma + z V_\Gamma u^s|_\Gamma - V_\Gamma g^{ext}, \quad \mathbf{x} \in \Gamma. \end{aligned}$$

This can be compactly expressed in terms of set equality on Γ by dropping the $\mathbf{x}$ dependence and reorganizing:

$$\left(K_\Gamma + zV_\Gamma - \frac{1}{2}I_\Gamma\right) u^s|_\Gamma = V_\Gamma g^{ext},$$

and so we have that:

$$u^s|_\Gamma = \left(K_\Gamma + zV_\Gamma - \frac{1}{2}I_\Gamma\right)^{-1} V_\Gamma g^{ext}.$$

From the last equation, we can identify $\mathcal{S}^{Ext}$ as being:

$$\mathcal{S}^{Ext} = I_\Gamma - 2z\left(K_\Gamma + zV_\Gamma - \frac{1}{2}I_\Gamma\right)^{-1} V_\Gamma.$$

□

CHAPTER 5

NUMERICAL TREATMENT OF BOUNDARY INTEGRAL EQUATIONS

5.1 A Brief Review of Quadrature Rules

Adopting a BIE approach to solve the Helmholtz problem is most likely paired with a choice of quadrature rule for the underlying integral, a process called Nystrom discretization. From the Green's representation, or more generally from acoustic layer potentials combinations, one obtains second-kind BIEs of the form:

$$\varphi(t) + \int_0^T K(t,\tau)\varphi(\tau)d\tau = f(t), \quad t \in [0,T],$$

where $K(t,\tau)$ is a doubly periodic kernel with always at least a logarithmic singularity about the diagonal $t = \tau$. For the most part, the resulting weakly singular integrals do not pose any issue in practice as there are quite a few methods available to deal with them and even offer provision for the more sensitive hypersingular case. These methods essentially fall into two categories depending on whether the kernel is splitted so that the log singularity is exposed explicitly or not. Amongst the popular methods that address this singularity, we have:

1. **Kapur-Rokhlin** (No split) : A trapezoid rule method where only the weights are modified near the diagonal.
2. **Alpert** (No split) : A trapezoid rule method where the equidistant nodes location near the diagonal are carefully replaced by optimal ones.
3. **Modified Gaussian** (No split) : A Gauss-Legendre panels rule where auxiliary nodes are added to each target nodes. These new nodes are selected using the Kolm-Rokhlin algorithm.
4. **Kress** (Explicit split) : This spectrally convergent method is the one we use in this work and consist of creating a kernel split so as to expose explicitly the

logarithmic singularity:

$$K(t,\tau) = K_1(t,\tau)\ln\left(4\sin^2\left(\frac{t-\tau}{2}\right)\right) + K_2(t,\tau),$$

for some K_1, K_2 smooth functions. The two quantities are then integrated using a periodic trapezoid rule and a product quadrature rule, respectively.

In Chapter 2, we have derived expressions to the radiative solution for the exterior scattering problem, both for open and closed boundary. Furthermore, it was established that in order to evaluate that solution at a given field point $\mathbf{x}$, one first needs to solve a boundary integral equation for an unknown density φ. We recall here that the two integral equations that need to be solved are of the form:

$$\varphi(\mathbf{x}) + 2\int_{\partial S}\left\{\frac{\partial G_k(\mathbf{x}-\mathbf{y})}{\partial \mathbf{n}(\mathbf{x})} - i\eta G_k(\mathbf{x}-\mathbf{y})\right\}\varphi(\mathbf{y})ds(\mathbf{y}) = b(\mathbf{x}), \quad \mathbf{x}\in\partial S,$$

when the boundary is closed and:

$$\int_{\Gamma} G_k(\mathbf{x}-\mathbf{y})\varphi(\mathbf{y})ds(\mathbf{y}) = b(\mathbf{x}), \quad \mathbf{x}\in\Gamma,$$

for an open boundary. Of particular interest to us is the fact that in both cases, the kernels are weakly singular with logarithmic singularities as $\mathbf{x}\to\mathbf{y}$ of the form $\ln\frac{k|\mathbf{x}-\mathbf{y}|}{2}$. With that in mind, we choose to develop the numerical procedure for a general kernel $K(\mathbf{x},\mathbf{y})$ with the same kind of singularity. We will, however, need to treat the case for open boundary in its own right since the results for closed boundary are not readily applicable, mostly due to the fact that the high order accuracy that we will claim relies exclusively on the assumed periodicity of the quantities involved.

5.2 The Quadrature Rule for Integrals with Periodic Boundaries

Let ∂S be the 2π-periodic boundary of a closed scatterer S with parametrization $\mathbf{y}(t) = (y_1(t), y_2(t))$ such that $\mathbf{y}([0, 2\pi)) = \partial S$. Noting that for $\mathbf{x} \in \partial S$, there must be a $t \in [0, 2\pi)$ satisfying $\mathbf{x} = \mathbf{y}(t)$, we shall abuse notation slightly in the following by letting $K(\mathbf{x}, \mathbf{y}) = K(\mathbf{y}(t), \mathbf{y}(\tau)) =: K(t, \tau)$ and similarly $\varphi(\mathbf{y}) =: \varphi(\tau)$ and so forth, should we encounter other such quantities. Our goal is to solve numerically the following Fredholm equation of the second type:

$$\varphi(t) + \int_0^{2\pi} K(t, \tau)\varphi(\tau)d\tau = b(t), \quad t \in [0, 2\pi), \tag{5.1}$$

where the kernel is assumed to be weakly singular as $t \to \tau$ with decomposition:

$$K(t, \tau) = K_1(t, \tau) \ln \frac{k|\mathbf{y}(t) - \mathbf{y}(\tau)|}{2} + K_2(t, \tau),$$

for some (doubly) periodic and analytic functions K_1, K_2.

While in general, there is no closed-form solution to the integral equation (5.1), we can nonetheless find a good (convergent) numerical approximation. Nyström method consists of selecting a quadrature rule to evaluate the integral and then solving the resulting square system.

To be precise, if we let $\{t_j = j\pi/n : j = 0, ..., 2n - 1\}$ be an equi-spaced partition of $[0, 2\pi)$, $\varphi_i := \varphi(t_i)$, and $b_i := b(t_i)$ for $i = 0, ..., 2n - 1$, the Nyström method consists of constructing a matrix A such that:

$$A\boldsymbol{\varphi}^{(n)} = \boldsymbol{b} \quad \text{with } \boldsymbol{b}, \boldsymbol{\varphi}^{(n)} \in \mathbb{R}^{2n}, \quad A \in \mathbb{R}^{2n \times 2n},$$

where the action of the square matrix A is "close" to that of the integral operator $I + \int K(\cdot)d\tau$. The matrix A will be determined by our choice of quadrature rule to evaluate equation (5.1) numerically. In a general setting, if we choose the following quadrature rule:

$$\int_0^{2\pi} K(t_i, \tau)\varphi(\tau)d\tau \approx \sum_{j=0}^{2n-1} \left(w_{ij}K(t_i, t_j)\right)\varphi_j,$$

then the matrix A is:

$$[A]_{ij} = 1 + w_{ij}K(t_i, t_j).$$

When we can construct such a matrix A, the numerical approximation of φ is given by:

$$\boldsymbol{\varphi}^{(n)} = A^{-1}\boldsymbol{b},$$

and for any t that is not contained on the partition, interpolation can be used.

In order to derive a high order quadrature rule, we need to deal with the singularity of the kernel. For that purpose, we review the Nyström quadrature rule presented in Colton & Kress [30] with additional insights and explanations, which I hope will benefit the reader. We still wish to solve the following BIE:

$$\varphi(t) + \int_0^{2\pi} \left(K_1(t, \tau)\ln\frac{k|\mathbf{y}(t) - \mathbf{y}(\tau)|}{2} + K_2(t, \tau)\right)\varphi(\tau)d\tau = b(t), \quad t \in [0, 2\pi).$$

For reasons that will be soon apparent, we proceed with a so-called kernel split:

$$\begin{aligned}\ln\left(\frac{k}{2}|\mathbf{y}(t)-\mathbf{y}(\tau)|\right) &= \ln\left(\frac{k}{2}\frac{|\mathbf{y}(t)-\mathbf{y}(\tau)|}{|t-\tau|}\right)\\ &+ \ln\left(\frac{|t-\tau|}{2\sin\left(\frac{|t-\tau|}{2}\right)}\right)\\ &+ \frac{1}{2}\ln\left(4\sin^2\left(\frac{t-\tau}{2}\right)\right).\end{aligned}$$

The first two terms on the right-hand side are not singular as $t \to \tau$ and have combined limit $\ln\left(\frac{k}{2}|\mathbf{y}'(t)|\right)$, and the last quantity is a 2π-periodic quantity. In light of the last development, the following updated, but totally equivalent, kernel split will be used.

$$K(t,\tau) = \widetilde{K}_1(t,\tau)\ln\left(4\sin^2\left(\frac{t-\tau}{2}\right)\right) + \widetilde{K}_2(t,\tau),$$

We identify $\widetilde{K}_1 = \frac{1}{2}K_1$ and $\widetilde{K}_2 = K - K_1\ln\left(4\sin^2\left(\frac{t-\tau}{2}\right)\right)$ with limiting value $\widetilde{K}_2(t,t) = K_2(t,t) + K_1(t,t)\ln\left(\frac{k}{2}|\mathbf{y}'(t)|\right)$. Hence the problem is now reduced to evaluating the following two integrals:

- $I_1 := \int_0^{2\pi} \ln 4\sin^2\left(\frac{t-\tau}{2}\right) f(\tau)d\tau$,
- $I_2 := \int_0^{2\pi} f(\tau)d\tau$,

for some smooth and 2π-periodic function f.

For I_2, the periodic trapezoidal rule is used due to its spectral convergence when dealing with smooth periodic functions:

$$I_2 \approx \frac{\pi}{n}\sum_{j=0}^{2n-1} f(t_j).$$

The first integral I_1 requires more work. The approximation that is detailed next falls in the category of product quadrature rules. A product quadrature rule approximates the integral of the product of two 2π-periodic functions g and f, where f is assumed to be smooth and g is real and allowed to be singular, as is the case here.

$$\int_0^{2\pi} f(\tau)g(\tau)d\tau \approx \sum_{j=0}^{2n-1} w_j f(t_j).$$

To obtain the weights, we start by assuming that both f and g have convergent Fourier series:

$$f(\tau) = \sum_{m\in\mathbb{Z}} f_m e^{in\tau},$$
$$g(\tau) = \sum_{m\in\mathbb{Z}} g_m e^{in\tau},$$

with Fourier coefficients:

$$f_m = \frac{1}{2\pi}\int_0^{2\pi} e^{-im\tau} f(\tau)d\tau \quad \text{and } g_m = \frac{1}{2\pi}\int_0^{2\pi} e^{-im\tau} g(\tau)d\tau.$$

From Parseval's theorem, we know that for such convergent representations:

$$\int_0^{2\pi} f(\tau)\overline{g(\tau)}d\tau = 2\pi\sum_{m\in\mathbb{Z}} f_m\overline{g_m} \approx 2\pi \sum_{-n\le m\le n}{}' f_m\overline{g_m},$$

which holds to high accuracy for rapidly decaying coefficients. The prime on the sum indicates that the first and last terms are being halved.

Next, the Fourier coefficients of f and $g = \ln 4\sin^2\left(\frac{t-\tau}{2}\right)$ are computed with ease observing that for this choice of g, they are known exactly. The following

proposition encapsulates this result and tells us a bit more that we will need later on.

Proposition 1.

$$\int_0^{\pi} \ln 4\sin^2\left(\frac{\tau}{2}\right) e^{-im\tau} d\tau = \int_{\pi}^{2\pi} \ln 4\sin^2\left(\frac{\tau}{2}\right) e^{-im\tau} d\tau = \begin{cases} 0 & m = 0 \\ -\frac{\pi}{|m|} & |m| = 1, 2, 3, \ldots \end{cases}$$

In particular, if any of the integrals on the LHS is from 0 *to* 2π*, then the RHS is multiplied by* 2*.*

Hence, for $g(\tau) = \ln\left(4\sin^2\left(\frac{t-\tau}{2}\right)\right)$, a change of variable gives $g_m = -\frac{e^{-imt}}{|m|}$. As for the coefficients f_m, we know that for smooth and 2π-periodic functions the best quadrature rule that we have is the periodic trapezoid rule with spectral accuracy:

$$f_m = \frac{1}{2\pi}\int_0^{2\pi} e^{-im\tau} f(\tau) d\tau \approx \frac{1}{2n}\sum_{j=0}^{2n-1} e^{-imt_j} f(t_j).$$

Having found the Fourier coefficients, we truncate the Parseval's identity and find:

$$\begin{aligned} I_1 &\approx 2\pi \sum_{0<|m|\leq n}{}' \left(\frac{1}{2n}\sum_{j=0}^{2n-1} e^{-imt_j} f(t_j)\right)\left(-\frac{\overline{e^{-imt}}}{|m|}\right) \\ &= -\frac{\pi}{n}\sum_{j=0}^{2n-1} \sum_{0<|m|\leq n}{}' \frac{e^{-im(t_j - t)}}{|m|} f(t_j) \\ &= \sum_{j=0}^{2n-1} R_j^{(n)}(t) f(t_j), \end{aligned}$$

where the coefficients $R_j^(n)(t)$ are obtained through the use of $e^{it} + e^{-it} = 2\cos t$ and are:

$$R_j^{(n)}(t) := -\frac{2\pi}{n} \sum_{m=1}^{n-1} \frac{\cos(m(t-t_j))}{m} - \frac{\pi}{n^2} \cos(n(t-t_j)).$$

Putting these two quadrature rules together in the integral equation gives us the linear system:

$$\varphi_i + \sum_{j=0}^{2n-1} \left\{ R_j^{(n)}(t_i) \widetilde{K}_1(t_i, t_j) + \frac{\pi}{n} \widetilde{K}_2(t_i, t_j) \right\} \varphi_j = b(t_i) \quad i = 0, ..., 2n-1.$$

Accordingly, the matrix A that we seek is given by:

$$[A]_{ij} = 1 + \left\{ R_j^{(n)}(t_i) \widetilde{K}_1(t_i, t_j) + \frac{\pi}{n} \widetilde{K}_2(t_i, t_j) \right\}.$$

We can now apply this method to our problem with $K(t,\tau) = \frac{i}{4} H_0^1(k|\mathbf{y}(t) - \mathbf{y}(\tau)|)$. All is needed is to use:

- $\widetilde{K}_1(t,\tau) = -\frac{1}{4\pi} J_0(k|\mathbf{y}(t) - \mathbf{y}(\tau)|)$,
- $\widetilde{K}_2(t,\tau) = K(t,\tau) - \ln 4 \sin^2\left(\frac{t-\tau}{2}\right) \widetilde{K}_1(t,\tau)$ and
- $\widetilde{K}_2(t,t) = \frac{i}{4} - \frac{\gamma}{2\pi} - \frac{1}{2\pi} \ln \frac{k|\mathbf{y}'(t)|}{2}$.

In practice, the field is evaluated using the same mesh with the trapezoid rule.

5.3 The Quadrature Rule for Integrals with non Periodic Boundaries

In this section, we are concerned with solving a Fredholm Equation of the first kind where as before, we will work with a general kernel $K(x, y) = K(t, \tau)$ which exhibit a log singularity like $\ln \frac{k|x-y|}{2}$ as $x \to y$.

$$\int_0^{2\pi} K(t,\tau)\phi(\tau)d\tau = -u^{inc}(\mathbf{y}(t)), \quad t \in [0, 2\pi].$$

The key differences here are (1) the density φ is no longer smooth (it actually blows up like $\sqrt{d}$ where d is the distance to the end-points of the arc) and (2) the quantities φ are no longer 2π-periodic (since the obstacle is open). The high order rule that we just presented would not be of high order here, but only as fast as the decay of the Fourier coefficients for a non-smooth/non- periodic function.

This issue is remedied by the introduction of the sigmoid transform $w : [0, 2\pi] \to [0, 2\pi]$ which turns an equispaced mesh into a mesh with agglomerations at the end-points of the interval on account that w' vanishes exponentially at either end as $\tau \to 0^+$ and $\tau \to 2\pi^-$. The one proposed in Colton & Kress is:

$$w(s) = 2\pi \frac{[v(s)]^p}{[v(s)]^p + [v(2\pi - s)]^p}, \quad 0 \le s \le 2\pi,$$

where

$$v(s) = \left(\frac{1}{p} - \frac{1}{2}\right)\left(\frac{\pi - s}{\pi}\right) + \frac{1}{p}\frac{s - \pi}{\pi} + \frac{1}{2}.$$

The integral remains mostly unchanged although we can recognize periodic quantities as shown in the following. Letting $\tau = w(s)$ and $t = w(\xi)$ we have:

$$\begin{aligned}\int_0^{2\pi} K(t,\tau)\phi(\tau)d\tau &= \int_0^{2\pi} K(w(\xi),w(s))\phi(w(s))|w'(s)|ds \\ &= \int_0^{2\pi} K(\xi,s)\phi^w(s)ds,\end{aligned}$$

where the quantity $\phi^w(s) := \phi(w(s))|w'(s)|$ is now seen to be 2π periodic and *smooth*. The quadrature rule developed in Section 5.2 can readily be applied using the new set of points $\left\{w\left(\frac{j\pi}{n}\right)\right\}_{j=0}^{2n-1}$.

CHAPTER 6

NUMERICAL RESULTS

In this section, we present a variety of numerical results that highlight the performance of our Schur complement DDM algorithm for solution of multiple scattering problems. All the results presented here were produced on a quad core (3.7 GHz Intel Xeon processor) Mac Pro machine with 64Gb of memory by a MATLAB implementation of our algorithm. We present results for scattering from clouds of sound-soft scatterers (e.g., Dirichlet boundary conditions on the scatterers). The extension to other types of boundary conditions is straightforward. We create clouds of scatterers by choosing a large box that we subdivide into L subdomains (boxes) and then we place inside each subdomain P scatterers whose position is random, while ensuring that the scatterers do not intersect each other and do not intersect the boundary of the domain.

Our DD algorithm proceeds in two stages: an offline (precomputation) stage whereby all the subdomain RtR maps are computed using the Nyström discretization presented in Chapter 4, and a stage where the DDM linear system is solved via hierarchical Schur complements. Finally, in the solution stage, we solve a linear system involving a dense matrix that corresponds to connecting the unknowns on the inner/outer artificial boundary through interior and respectively exterior RtR maps. We note that although the algorithm is highly parallelizable, our current implementation does not take advantage of these possibilities.

We comment next on the computational complexity of our Schur complement elimination algorithm. Assuming a collection of $L = \ell_1 \times \ell_2$ of identical square subdomains, each one containing P_L scatterers inside. If n_P collocation points are used per each scatterer to resolve the solution (say that these amount to 6 pts/wavelength which is typical for Nyström discretizations of boundary integral

equations) then we argue that about $P_L^{1/2} n_P^{1/2}$ collocation points are needed per side of each subdomain. Since there are overall $2\ell_1\ell_2 + \ell_1 + \ell_2$ common interfaces in the DD algorithm, the discretization of the DDM linear system would require about $2(2\ell_1\ell_2 + \ell_1 + \ell_2) P_L^{1/2} n_P^{1/2}$ unknowns (recall that there are two unknowns per interface). However, the matrix corresponding to the DDM linear system, although sparse, is never stored in practice, and the solution of that system is performed by employing hierarchical Schur complements of small size. The cost of our Schur complement elimination algorithm is thus dominated by that of the solution of the DDM linear system that features a dense matrix corresponding to unknowns on the inner/outer interface, and as such the cost is $\mathcal{O}((2(\ell_1 + \ell_2) P_L^{1/2} n_P^{1/2})^3)$. Thus, if we denote $N_T = \ell_1\ell_2 P_L n_P$, the computational cost of our Schur complement solver is roughly $\mathcal{O}((4N_T)^{3/2})$. In addition, the precomputation/offline stage of our algorithm requires a computational cost of $\mathcal{O}(\ell_1\ell_2(P_L n_P)^3)$ in order to compute the L subdomain RtR maps, assuming that the distribution of scatterers inside each box is different. Nevertheless, in the important case of photonic crystal applications (the centers of the scatterers occupy the vertices of a finite lattice), the distribution of scatterers inside the subdomains is identical, in which instance the precomputation cost can be significantly reduced. The cost of computing a single subdomain RtR map can be further reduced if fast compression algorithms such as $\mathcal{H}$-matrices are used. In contrast, the cost of a direct boundary integral solver for the solution of the multiple scattering problem would be $\mathcal{O}(N_T^3)$ with a $\mathcal{O}(N_T^2)$ amount of memory needed. Consequently, in multiple scattering applications that involve very large numbers of scatterers, the direct approach is simply too costly. In case Krylov subspace iterative solvers are employed for the solution of the very large linear algebra problem resulting from the direct approach, the numbers of iterations is prohibitive. Clearly, our algorithm is competitive when the number of scatterers per subdomain (i.e. P_L) is large. We emphasize that our DD algorithm is a direct

method, and as such multiple incidence can be treated with virtually no additional cost.

We present in Table 6.1 a comparison between the global BIE approach and our DD algorithm. The multiple scattering configuration in this experiment consists of a cloud of 640 lines segment scatterers, a configuration that is challenging to volumetric discretizations (e.g., finite differences, finite elements). More precisely, our configuration is enclosed by a square box of size 16 by 16 which is divided in a collection of 4×4 subdomains, each a square box of size 4 in which we placed a collection of 40 line segments of length 0.4 whose centers and orientations are chosen randomly (yet avoiding self intersections and intersections with the boundary of the box). The distribution of scatterers is different in each subdomain, and thus the subdomain RtR maps are different. In all the numerical results presented, we report in the column "Unknowns" the total number of unknowns needed to discretize the scatterers in the cloud; in the column "Unknowns DD" we report the number of unknowns in the original DD linear system and the number of unknowns in the reduced system where we solve for the exterior Robin data. We emphasize that the matrix related to the DD system is not stored, it is only the matrix in the reduced system obtained after applications of the Schur complements that is stored. Our DD algorithm uses 4×4 subdomains. We chose a wavenumber $k = 8$ such that the scattering ensemble has size $20\lambda \times 20\lambda$ and we compared the far-field results produced by each method, and we observe excellent agreement. As it can be seen from the results in Table 6.1, our solver is more competitive than the solver based on the global first kind boundary integral equation (BIE) formulation of the multiple scattering problem, even when accounting for the offline cost. We present in Figure 6.1 a depiction of the total field in a neighborhood of the scatterer cloud.

Table 6.1 Comparison of Schur Complement DD Solver with a BIE Direct Solver.

Unknowns	BIE solver	Unknowns DD	Offline	DD			Error far-field
				Hierarchical elimination	Solution	Total time	
5,120	13.24	2,560/512	2.00	0.12	0.22	0.34	1.0×10^{-1}
10,240	66.56	3,840/768	5.90	0.18	0.47	1.05	3.1×10^{-3}
20,480	419.74	5,760/1,152	21.61	0.42	1.10	1.52	9.9×10^{-5}

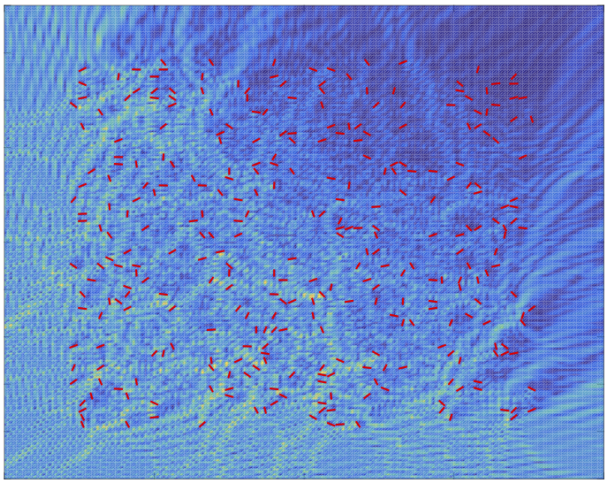

Figure 6.1 Total field scattered by a cloud of 160 line segments.

We present in Table 6.2 an illustration of the performance of our algorithm for large clouds of scatterers (e.g. made up of 10,240 and respectively 40,960 scatterers) that span domains of size $80\lambda \times 80\lambda$ and respectively $160\lambda \times 160\lambda$, each scatterer being of size 0.4λ. Again, the arrangement of scatterers in the subdomains was produced in the same manner as in Table 6.1 (there are 16×16 and respectively 32×32 subdomains), and the distribution of scatterers is different in each subdomain. These configurations could model rain drops or possibly foliage. Given the large size of the cloud, global BIE based methods are beyond the limits of the computational resources we used in these experiments. The number of collocation points used for the discretization of the RtR maps was chosen to be $\mathcal{O}(N_T^{1/2})$ where N_T is the number of discretization points needed on the scatterers. We present in Figure 6.2 Radar Cross Section (RCS) plots (in dB) for (a) the configuration used in Table 6.2 and (b) for the same geometric arrangement but doubling the frequency (this makes the cloud of scatterers to span a domain of size $160\lambda \times 1600\lambda$) when a plane wave

Table 6.2 Performance of Schur Complement DD Solver for many Configurations.

Size	Unknowns	Unknowns DD	Offline	DD			Error far-field
				Hierarchical elimination	Solution	Total time	
$10{,}240/80\lambda \times 80\lambda$	81,920	34,816/2,048	26.6	3.2	4.1	7.3	7.3×10^{-1}
$10{,}240/80\lambda \times 80\lambda$	163,840	52,224/3,072	88.9	8.9	10.6	19.5	6.5×10^{-2}
$10{,}240/80\lambda \times 80\lambda$	327,680	78,336/4,608	337.1	25.4	30.4	55.8	6.9×10^{-3}
$10{,}240/80\lambda \times 80\lambda$	655,360	117,504/6,912	1,388	79.7	85.1	164.8	4.2×10^{-6}
$40{,}960/160\lambda \times 160\lambda$	1,310,720	304,128/6,144	1,473	208.1	197.8	405.9	6.4×10^{-3}

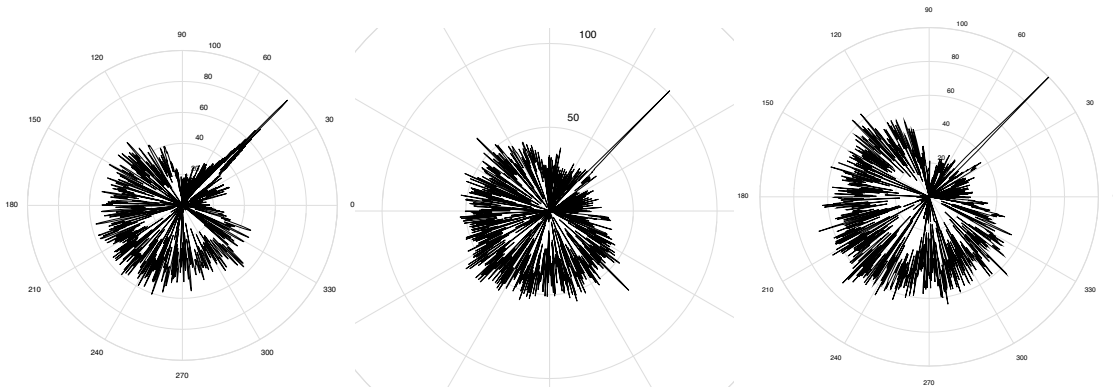

Figure 6.2 Radar cross sections (RCS) from a large cloud of scatterers for a 45 degree incident field.

whose direction is making a 45° angle with the vertical impinges on the ensemble of scatterers. From left to right, we detail: (a) $80\lambda \times 80\lambda$ (left), each scatterer is about 0.4λ; (b) $160\lambda \times 160\lambda$ (center), each scatterer is about 0.8λ; and (c) 40,960 line segment scatterers occupying a region of size $160\lambda \times 160\lambda$ (right), each scatterer is about 0.4λ.

If we use the DD-ABC algorithm (and thus the solution stage is no longer needed) for the configurations presented in Table 6.2, we obtain results with relative errors of about 7% in the far field (the boundary of the enclosing box ∂B_0 is placed about 1λ away from the collection of scatterers).

We conclude with an illustration in Figure 6.3 of the performance of our DD solver for simulation of wave propagation in photonic crystal like structures such as those depicted in that figure. More specifically, the geometric configuration consists

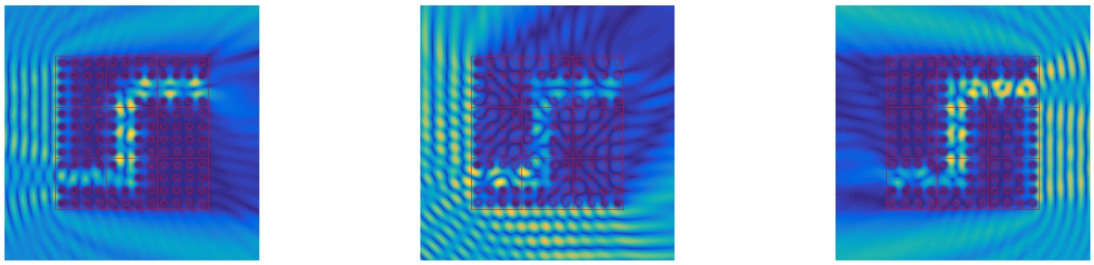

Figure 6.3 Simulation of propagation through a channel defect.

of a finite yet large collection of circles such that the distances between them equal their diameter in which a channel defect is created. The width of the channel equals three times the diameter of the circles. We considered plane wave incident fields with different directions of propagation and a wavelength such that the size of each scatterer is 0.6λ. In such configurations the most natural DD strategy is to have two types of subdomains, one containing precisely one scatterer inside, and one that does not contain scatterers inside. In this manner, only two subdomain RtR maps need be computed. Using 16 discretization points per scatterer and 64 discretization points on the boundary of each subdomain, the computational times required by our Schur complement DD algorithm to simulate wave propagation in structures like that depicted in Figure 6.3 containing collections of $20 \times 20, 40 \times 40, 60 \times 60, 80 \times 80$, and 100×100 scatterers are respectively $6.1, 46.7, 234.6, 463.1$ and 1075 seconds.

6.1 Validation of the Foldy-Lax Approximation

As we pointed out earlier, an approximation scheme that is well suited for the multiple scattering problem by a large ensemble of randomly positioned arc segments is the Foldy-Lax method. The error tracking of such methods has historically been hard to achieve as direct solvers would choke on big configurations. Our DDM formulation now allows to validate the approximation for such configurations that were so far out of reach by exact methods. We briefly review what the Foldy-Lax approximation entails and close this section with convincing results.

The Foldy-Lax method is a solution technique for multiple scattering problems where the scatterers are assumed to be isotropic point scatterers. Hence, in this setup consider a collection of m isotropic point scatterers in the plane with positions $\{\mathbf{x}_j\}_{j=1}^m$. It is natural to expect, especially when recalling that the Green's function is the response to a point source of unit strength, that the field be expressed as sum over all point sources.

$$u^s(\mathbf{x}) = \sum_{j=1}^{m} A_j G_k(\mathbf{x} - \mathbf{x}_j),$$

where the A_j are meant to capture in some way the intensity of each point source. When evaluating the field on a scatterer, say $u^s(\mathbf{x}_n)$, it is intuitive that the response ought to be the sum of all other contributions, leaving out the term corresponding to that scatterer, which is written:

$$u_n := u^s(\mathbf{x}_n) = \sum_{j \neq n} A_j G_k(\mathbf{x}_n - \mathbf{x}_j), \quad n = 1, ..., m.$$

This system is not uniquely solvable since there are two set of unknowns $\{u_j\}_{j=1}^m$ and $\{A_j\}_{j=1}^m$. In light of this observation, the Foldy-Lax method suggests the use of $A_j = \sigma_j u_j$ where the σ_j are some sort of intensity coefficients specific to each scatterers and for more details on how to evaluate them we refer to Martin [22]. For scatterers that have a size to them, a fair approximation is to relate their intensity coefficient to their diameter, which loosely speaking amounts to treating them as the smallest ball in which they can be enclosed.

The ones that were used here are given by

$$\sigma_j = -i\lambda_j(1 + i\lambda_j)^{-1},$$

where

$$\lambda_j = -\frac{\pi}{2}\left\{\ln\left(\frac{kd_j}{4}\right) + \gamma\right\}^{-1},$$

and where d_j is the diameter of the j^{th} scatterer and $\gamma = 0.5772...$ is the Euler constant introduced before.

With this approximation no distinction is made between two line segments of the same length but orthogonal to each others - which at first makes little sense as one of the lines may reflect all the incident field while the other shouldn't reflect anything. However, our tests beg to differ that when the method is used for a large ensemble of line scatterers with random positions and orientations, the approximation is surprisingly good. As our results point out, when we double the size of the ensemble, the error in the far field over all directions stays roughly the same, which makes this approximation particularly attracting for very, very large problems where only our method can cope with in an exact matter.

That this approximation gets better as the size of the ensemble of random scatterers increases hints that some sort of averaging out is happening and further suggests that research into probabilistic methods for this kind of problem would not be a bad idea. When enforcing this assumption, we get the linear system for the total field $u = u^s + u^{inc}$:

$$u_n + u^{inc}(\mathbf{x}_n) = \sum_{j \neq n} \sigma_j u_j G_k(\mathbf{x}_n - \mathbf{x}_j), \quad n = 1, ..., m,$$

which in matrix notation,

$$\begin{bmatrix} 1 & -\sigma_2 G_k(\mathbf{x}_1-\mathbf{x}_2) & \cdots & -\sigma_m G_k(\mathbf{x}_1-\mathbf{x}_m) \\ -\sigma_1 G_k(\mathbf{x}_2-\mathbf{x}_1) & 1 & \cdots & -\sigma_m G_k(\mathbf{x}_2-\mathbf{x}_m) \\ \vdots & \vdots & \ddots & \vdots \\ -\sigma_1 G_k(\mathbf{x}_m-\mathbf{x}_1) & -\sigma_2 G_k(\mathbf{x}_m-\mathbf{x}_2) & \cdots & 1 \end{bmatrix} \begin{bmatrix} u_1 \\ u_2 \\ \vdots \\ u_m \end{bmatrix} = \begin{bmatrix} u^{inc}(\mathbf{x}_1) \\ u^{inc}(\mathbf{x}_2) \\ \vdots \\ u^{inc}(\mathbf{x}_m) \end{bmatrix}.$$

The far field in direction $\hat{\mathbf{x}} = \frac{\mathbf{x}}{|\mathbf{x}|}$ can then be computed easily through

$$u^{s,\infty} = \frac{e^{i\pi/4}}{\sqrt{8\pi k}} \sum_{j=1}^{m} \sigma_j u_j e^{-ik\hat{\mathbf{x}}\cdot\mathbf{x}_j}.$$

We give an overview of a few tests that we have conducted using the Foldy-Lax approximation to see how well it would cope with open arc agglomerations. As Figure 6.4 suggests, Foldy-Lax seems to perform adequately keeping in mind that it is an extremely simplified approximation. Most importantly is the times, not reported here, that were the most impressive. Foldy-Lax method only uses one point per scatterer hence reducing tremendously the computation efforts so that in all three cases the computation times where nearly instantaneous on a personal laptop with an i5 dual core CPU.

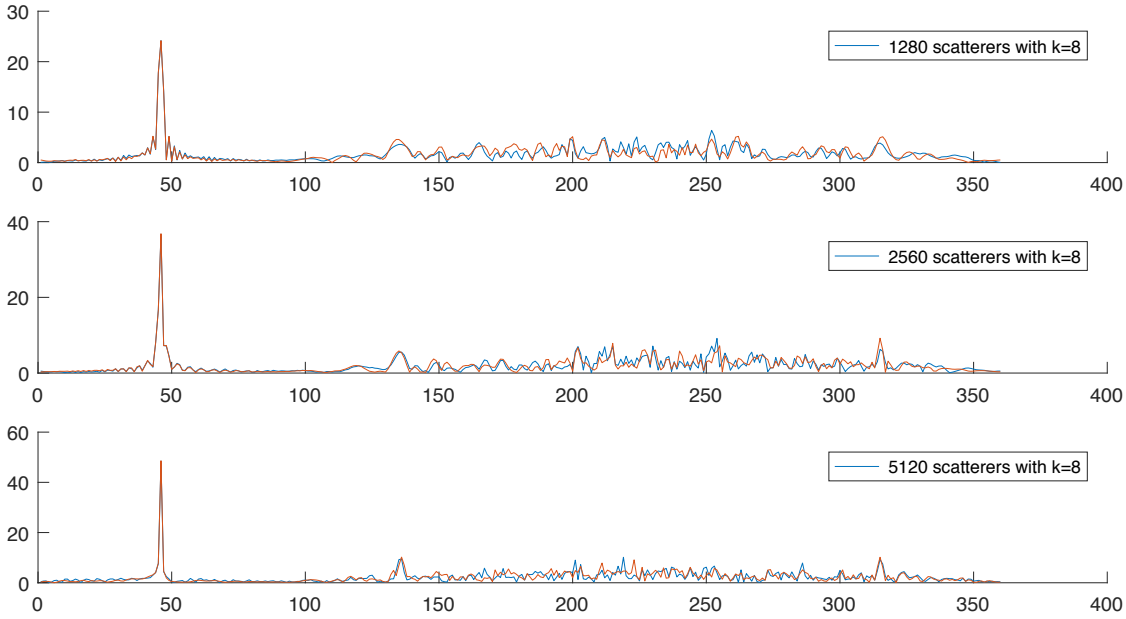

Figure 6.4 Comparison of Foldy-Lax and DDM for far field readings in all directions.

APPENDIX

CONSTRUCTION OF THE 2D HELMHOLTZ GREEN'S FUNCTION

The fundamental solution $G_k(\mathbf{x}, \mathbf{y}) := G_k(\mathbf{x} - \mathbf{y})$ satisfies

$$\Delta G_k + k^2 G_k = \delta(\mathbf{x} - \mathbf{y}) \qquad \mathbf{x}, \mathbf{y} \in \mathbb{R}^2$$
$$\lim_{|\mathbf{x}| \to \infty} |\mathbf{x}|^{\frac{1}{2}} \left(\frac{\partial G}{\partial |\mathbf{x}|} - ikG \right) = 0$$

where $\Delta = \frac{\partial^2}{\partial x_1^2} + \frac{\partial^2}{\partial x_2^2}$.

We can see from the above PDE that $G_k(\mathbf{x} - \mathbf{y})$ does not depend on any geometry in the plane, but rather seems to only be concerned with how far $\mathbf{x}$ is located away from $\mathbf{y}$. This should not be surprising when we recall that the physical interpretation of the fundamental solution is the response at the field point $\mathbf{x}$ to a point source located at $\mathbf{y}$ with unit strength. For this reason, we will seek a solution in terms of $r = |\mathbf{x} - \mathbf{y}|$. We effect this in the following development through the use of $g(r) = G_k(\mathbf{x} - \mathbf{y})$.

The introduction of the polar coordinate $r = |\mathbf{x} - \mathbf{y}|$ requires to migrate the operator $\Delta + k^2$ to polar coordinates. Because there seem to be no angular dependence, we can quite easily find the polar counterpart of $\Delta = \frac{\partial^2}{\partial x_1^2} + \frac{\partial^2}{\partial x_2^2}$ by first computing, using the chain rule $\nabla G_k = g' \nabla r = g' \frac{\mathbf{x} - \mathbf{y}}{r}$, followed by a use of the

product rule

$$\begin{aligned}\Delta G_k &= \nabla \cdot \nabla G_k \\ &= \nabla \cdot (g' \nabla r) \\ &= \nabla g' \cdot \nabla r + g' \nabla \cdot \nabla r \\ &= g'' \nabla r \cdot \nabla r + g' \nabla \cdot \nabla r \\ &= g'' |\nabla r|^2 + g' \Delta r\end{aligned}$$

From $\nabla r = \frac{\mathbf{x}-\mathbf{y}}{r}$, we see that $|\nabla r|^2 = 1$ and that by an application of the quotient rule

$$\begin{aligned}\Delta r &= \nabla \cdot \frac{\mathbf{x}-\mathbf{y}}{r} \\ &= \frac{r \nabla \cdot (\mathbf{x}-\mathbf{y}) - (\mathbf{x}-\mathbf{y}) \nabla r}{r^2} \\ &= \frac{2r - \frac{r^2}{r}}{r^2} = \frac{1}{r}.\end{aligned}$$

This shows that with no angular dependence, the Laplacian reduces to $\Delta = \frac{d^2}{dr^2} + \frac{1}{r}\frac{d}{dr}$. Putting everything together we now set to solve the following problem.

$$\begin{aligned} g'' + \frac{1}{r} g' + k^2 g = 0 \qquad & r > 0 \\ \lim_{r \to \infty} r^{\frac{1}{2}} \left(\frac{dg}{dr} - ikg \right) = 0 & \end{aligned}$$

This is an ODE that we can solve without any high machinery. We first note that the differential equation has a regular singular point at $r = 0$, namely the coefficient $\frac{1}{r}$ has a first order pole there which tells us that the solution will not be

analytic at the origin and that in turn, we should expect at least one solution of the Frobenius type

$$g_1(r) = r^q \sum_{j=0}^{\infty} a_j r^j \tag{1}$$

where $a_0 \neq 0$ and q is a constant which may be complex.

This expression can be somewhat simplified by multiplying through by r^2 and then making the change of variable $\rho = kr$ to get the following ODE, which is the well-known 0-th order Bessel equation.

$$\rho^2 g'' + \rho g' + \rho^2 g = 0 \qquad \rho > 0 \tag{2}$$

The next step is to replace the Frobenius representation (1) into (2) . We compute:

- $\rho^2 g_1''(\rho) = \rho^q \sum_{j=0}^{\infty} (j+q)(j+q-1) a_j \rho^j$
- $\rho g_1'(\rho) = \rho^q \sum_{j=0}^{\infty} (j+q) a_j \rho^j$
- $\rho^2 g_1(\rho) = \rho^q \sum_{j=0}^{\infty} a_j \rho^{j+2} = \rho^q \sum_{j=2}^{\infty} a_{j-2} \rho^j$

We can then add these three terms and divide through by ρ^q to obtain the following equation:

$$a_0 q^2 + a_1 (1+q)^2 \rho + \sum_{j=2}^{\infty} \left(a_j (j+q)^2 + a_{j-2} \right) \rho^j = 0$$

Since the only way that this equation can hold for all $\rho > 0$ is if all the coefficients are zero, we get a series of equations to solve for the coefficients. Starting with the indicial equation $q^2 = 0$, we readily get that $q = 0$ and when replaced in

the next coefficient it tells us that $a_1 = 0$. For $j = 2, 3, ...$ we obtain the recurrence relation

$$a_j = -\frac{1}{j^2} a_{j-2}$$

We note that since $a_1 = 0$, $a_j = 0$ whenever j is odd and for $j = 2m$, we find that

$$a_{2m} = -\frac{1}{(2m)^2} a_{2m-2} = (-1)^2 \frac{1}{(2m)^2(2m-2)^2} a_{2m-4} = ... = (-1)^m \frac{1}{2^{2m}(m!)^2} a_0.$$

For convenience, let us set $a_0 = 1$ and replace these coefficients in (1) to get that

$$g_1(\rho) = \sum_{m=0}^{\infty} (-1)^m \frac{1}{2^{2m}(m!)^2} \rho^{2m}$$

This is the Bessel function of the first kind of 0th order $J_0(\rho)$. Among other things, it has the property of being analytic everywhere (entire) which follows from an application of the ratio test, in particular at the origin. That the function is analytic at the origin already indicates that the second solution will be singular there.

In order to find that second solution, a good place to start is to use what we know of the equidimensional equation when the roots are repeated and try to feed the operator with a term like $\ln(\rho) g_1(\rho)$. Letting $L := \rho^2 \frac{d^2}{d\rho} + \rho \frac{d}{d\rho} + \rho^2$, straightforward differentiation shows that:

$$L[\ln(\rho) g_1(\rho)] = \ln(\rho) L_B[g_1] + 2\rho g_1' = 2\rho g_1'$$

We then seek an analytic function, say $F(\rho)$, such that $L[F] = -2\rho g_1'$, after which using the linearity of L, our second solution will be given by $g_2(\rho) = \ln(\rho)g_1(\rho) + F(\rho)$. If we let $F(\rho) = \sum_{m=0}^{\infty} b_m \rho^m$ and apply L to it we get to the following:

$$L[F] = b_1 x + \sum_{m=2}^{\infty} \left(b_m m^2 + b_{m-2}\right) \rho^m = -4 \sum_{m=1}^{\infty} m a_{2m} \rho^{2m} = -2\rho g_1'(\rho)$$

We can proceed with matching the coefficients of corresponding order and conclude that $b_1 = 0$ such that for odd powers of ρ,

$$b_{2m+1} = -\frac{1}{(2m+1)^2} b_{2m-1} = 0 \qquad m = 1, 2, 3, ...$$

and for even powers of ρ,

$$\begin{aligned}
b_{2m} &= -\frac{1}{(2m)^2} b_{2m-2} - \frac{1}{m} a_{2m} \\
&= -\frac{1}{(2m)^2} \left(-\frac{1}{(2m-2)^2} b_{2m-4} - \frac{1}{m-1} a_{2m-2} \right) - \frac{1}{m} a_{2m} \\
&= \frac{1}{2^4 (m(m-1))^2} b_{2m-4} + \frac{1}{m-1} \frac{a_{2m-2}}{(2m)^2} - \frac{1}{m} a_{2m} \\
&= \frac{1}{2^4 (m(m-1))^2} b_{2m-4} - a_{2m} \left(\frac{1}{m} + \frac{1}{m-1} \right) \\
&... \\
&= \frac{(-1)^{m+1}}{2^{2m} (m!)^2} b_0 - a_{2m} \left(\frac{1}{m} + \frac{1}{m-1} + ... + \frac{1}{2} \right) \\
&= -a_{2m}(b_0 - 1) - a_{2m} \sum_{i=1}^{m} \frac{1}{i} \\
&= -a_{2m}(b_0 - 1) - a_{2m} H_m
\end{aligned}$$

where H_m is the mth harmonic number. We therefore have an expression for $F(\rho)$:

$$\begin{aligned} F(\rho) &= b_0 + \sum_{m=1}^{\infty} b_{2m}\rho^{2m} \\ &= b_0 - (b_0 - 1)\sum_{m=1}^{\infty} a_{2m}\rho^{2m} - \sum_{m=1}^{\infty} a_{2m}H_m\rho^{2m} \\ &= b_0 - (b_0 - 1)(J_0(\rho) - 1) - \sum_{m=1}^{\infty} a_{2m}H_m\rho^{2m} \\ &= 2b_0 - 1 + J_0(\rho)(1 - b_0) - \sum_{m=1}^{\infty} a_{2m}H_m\rho^{2m} \end{aligned}$$

Since b_0 is arbitrary, we choose $b_0 = \frac{1}{2}$ to get rid of the constant, and we note that the J_0 term is a multiple of the first solution. Hence, the complete general solution to the Helmholtz equation that we are looking for takes the form

$$G_k(\mathbf{x} - \mathbf{y}) = AJ_0(kr) + B\left(\ln(kr)J_0(kr) - \sum_{m=1}^{\infty} a_{2m}H_m(kr)^{2m}\right)$$

where A, B are constants to determine.

The particular choice of constants $A = \frac{i}{4} - \frac{\gamma}{2\pi} + \frac{1}{2\pi}\ln 2$ and $B = -\frac{1}{2\pi}$, where $\gamma = \lim_{m\to\infty}(H_m - \ln m) = 0.5772...$ is the Euler Mascheroni constant, yield the Hankel form that is used in this text:

$$G_k(\mathbf{x} - \mathbf{y}) = \frac{i}{4}H_0^1(k|\mathbf{x} - \mathbf{y}|) = \frac{i}{4}(J_0(k|\mathbf{x} - \mathbf{y}|) + iY_0(k|\mathbf{x} - \mathbf{y}|))$$

where

$$Y_0(\rho) = \frac{2}{\pi}\left(\ln\frac{\rho}{2} + \gamma\right)J_0(\rho) - \frac{2}{\pi}\sum_{m=1}^{\infty} a_{2m}H_m\rho^{2m}$$

is called the Bessel function of the second kind of 0th order.

BIBLIOGRAPHY

[1] A. Anand, J. S. Ovall, and C. Turc. (2012). Testing boundary integral equations for two-dimensional sound-hard scattering problems in domains with corners. *Journal of Integral Equations and Applications*, 24(3), 321-358.

[2] X. Antoine, C. Chniti, and K. Ramdani. (2008). On the numerical approximation of high-frequency acoustic multiple scattering problems by circular cylinders. *Journal of Computational Physics*, 227(3), 1754-1771.

[3] X. Antoine, K. Ramdani, and B. Thierry. (2012). Wide frequency band numerical approaches for multiple scattering problems by disks. *Journal of Algorithms and Computational Technology*, 6(2), 241-260.

[4] N. Balin, A. Bendali, and F. Collino. (2005). Domain decomposition and additive schwarz techniques in the solution of a te model of the scattering by an electrically deep cavity. In *Domain Decomposition Methods in Science and Engineering*, Springer, 149-156.

[5] Y. Boubendir, X. Antoine, and C. Geuzaine. (2012). A quasi-optimal non-overlapping domain decomposition algorithm for the Helmholtz equation. *Journal of Computational Physics*, 231(2), 262-280.

[6] Y. Boubendir and C. Turc. (2013). Wave-number estimates for regularized combined field boundary integral operators in acoustic scattering problems with neumann boundary conditions. *IMA Journal of Numerical Analysis*, 33(4), 1176-1225.

[7] B. Després. (1990). Décomposition de domaine et problème de Helmholtz. *Comptes Rendus de l'Académie des Sciences - Series I - Mathematics*, 311(6), 313-316.

[8] V. Dominguez, M. Lyon, and C. Turc. (2015). Well-posed boundary integral equation formulations and Nystrom discretizations for the solution of Helmholtz transmission problems in two-dimensional lipschitz domains. *Journal of Integral Equations and Applications*, 28(3), 395-440.

[9] I. S. Duff and J. K. Reid. (1983). The multifrontal solution of indefinite sparse symmetric linear. *ACM Transactions on Mathematical Software*, 9(3), 302-325.

[10] S. Fliss, D. Klindworth, and K. Schmidt. (2015). Robin-to-Robin transparent boundary conditions for the computation of guided modes in photonic crystal wave-guides. *BIT Numerical Mathematics*, 55(1), 81-115.

[11] L. L. Foldy. (1945). The multiple scattering of waves I. General theory of isotropic scattering by randomly distributed scatterers. *Physical Review*, 67(3-4), 107-119.

[12] M. J. Gander, F. Magoulès, and F. Nataf. (2002). Optimized Schwarz methods without overlap for the Helmholtz equation. *SIAM Journal on Scientific Computing* , 24(1), 38-60.

[13] M. Ganesh, S. C. Hawkins, and R. Hiptmair. (2012). Convergence analysis with parameter estimates for a reduced basis acoustic scattering t-matrix method. *IMA Journal of Numerical Analysis*, 32(4), 1348-1374.

[14] A. George. (1973). Nested dissection of a regular finite element mesh. *SIAM Journal on Numerical Analysis*, 10(2), 345–363.

[15] S. Ghanemi, F. Collino, and P. Joly. (1995). Domain decomposition method for harmonic wave equations. *Mathematical and Numerical Aspects of Wave Propagation*, SIAM, 663-672.

[16] A. Gillman, A. H. Barnett, and P.-G. Martinsson. (2015). A spectrally accurate direct solution technique for frequency-domain scattering problems with variable media. *BIT Numerical Mathematics*, 55(1), 141-170.

[17] L. Gürel and W. C. Chew. (1992). A recursive T-matrix algorithm for strips and patches. *Radio science*, 27(3), 387–401.

[18] P. Joly, J.-R. Li, and S. Fliss. (2006). Exact boundary conditions for periodic waveguides containing a local perturbation. *Communications in Computational Physics*, 1(6), 945-973.

[19] D. A. Kopriva. (1998). A staggered-grid multidomain spectral method for the compressible Navier-Stokes equations. *Journal of Computational Physics*, 143(1), 125–158.

[20] J. Lai, M. Kobayashi, and L. Greengard. (2014). A fast solver for multi-particle scattering in a layered medium. *Optics express*, 22(17), 20481-20499.

[21] M. Lax. (1951). Multiple scattering of waves. *Reviews of Modern Physics*, 23(4), 287-310.

[22] P. A. Martin. (2006). *Multiple Scattering: Interaction of Time-Harmonic Waves with N Obstacles*, volume 107. Cambridge University Press.

[23] F. Montiel, V. A. Squire and L. G. Bennetts. (2015). Evolution of directional wave spectra through finite regular and randomly perturbed arrays of scatterers. *SIAM Journal of Applied Mathematics*, 75(2), 630-651.

[24] F. Nataf. (2001). Interface connections in domain decomposition methods. *Modern Methods in Scientific Computing and Applications. NATO Science Series II Mathematics, Physics and Chemistry*, vol 75. Springer, Dordrecht.

[25] A. N. Norris, A. J. Nagy and F. A. Amirkulova. (2013). Stable methods to solve the impedance matrix for radially inhomogeneous cylindrically anisotropic structures. *Journal of Sound and Vibration*, 332(10), 2520-2531.

[26] S. A. Orszag. (1980). Spectral methods for problems in complex geometries. *Journal of Computational Physics*, 37(1), 70-92.

[27] H. P. Pfeiffer, L. E. Kidder, M. A. Scheel and S. A. Teukolsky. (2003). A multidomain spectral method for solving elliptic equations. *Computer Physics Communications*, 152(3), 253-273.

[28] C. Turc, Y. Boubendir and M. K. Riahi. (2017). Well-conditioned boundary integral equation formulations and Nystrom discretizations for the solution of Helmholtz problems with impedance boundary conditions in two-dimensional lipschitz domains. *Journal of Integral Equations and Applications*, 29(3), 441-472.

[29] P. C. Waterman. (1965). Matrix formulation of electromagnetic scattering. *Proceedings of the IEEE*, 53(8), 805-812.

[30] D. Colton and R. Kress. (2013). *Inverse Acoustic and Electromagnetic Scattering Theory*, volume 93. Springer-Verlag New York.

[31] M. Pedneault, C. Turc and Y. Boubendir. (2017). Schur complement domain decomposition methods for the solution of multiple scattering problems. *IMA Journal of Applied Mathematics*, 82(5), 1104-1134.